Colloquium: Strong optical forces on atoms in multifrequency light

Harold Metcalf

Rev. Mod. Phys. **89**, 041001 — Published 19 October 2017

DOI: 10.1103/RevModPhys.89.041001

Strong Optical Forces on Atoms in Multi-frequency Light*

Harold Metcalf

Physics and Astronomy,
Stony Brook University,
Stony Brook NY 11794-3800

Abstract

Optical forces on atoms irradiated with a single frequency of light have been extensively studied for many years, both theoretically and experimentally. The two-level atom model has been used to describe a wide range of optical force phenomena and to exploit successfully a large range of applications. New areas of study were opened up when the multiple levels of real atoms were considered. In contrast, using multi-frequency light on a single atomic transition has not been studied as much, but using such light also results in very significant differences in the optical forces. This paper outlines the basic concepts of forces resulting from the use of two frequency light (bichromatic force) and swept frequency light (adiabatic rapid passage force). Both of these forces derive from stimulated processes only, and as a result can produce coherent exchange of momentum between atoms and light. The consequences are impressively larger forces with comparably larger velocity capture ranges, and even atom cooling without spontaneous emission.

CONTENTS

I. INTRODUCTION

A. Overview of Optical Forces

Ever since the time of Kepler, and perhaps even earlier, there were ideas of radiation pressure. Optical forces (light pressure) were derived by Maxwell who found that the force on an object absorbing P watts of light is $F = P/c$, and on a reflecting object is simply $F = 2P/c$. This result survived intact through the development of both relativity and quantum optics because $E = pc = \hbar\omega$, where p is momentum and $\omega = 2\pi\nu$ is frequency. Optical forces on macroscopic objects were demonstrated at the start of the 20^{th} century (Lebedev, 1901; Nichols and Hull, 1903), and on gases by (Lebedev, 1910). Light pressure was studied in the 1908 Ph.D. thesis of Peter Debye on comet tails.

The use of electromagnetic radiation to exert forces on individual neutral atoms was first demonstrated in 1933 (Frisch, 1933). The advent of stable, tunable lasers resulted in dramatic advances since that early time (Picqué and Vialle, 1972; Schieder *et al.*, 1972). A good review is found in (Mulser, 1985) and in the Nobel Lecture of Phillips (Phillips, 1998). The possibility of using such optical forces for controlling the motion and position of atoms was discussed in considerable detail in very many of the early papers of Ashkin (Ashkin, 1970, 1978; Ashkin and Gordon, 1983). The first cooling experiments that made a major change on the velocity distribution were done on trapped ions (Neuhauser *et al.*, 1978; Wineland *et al.*, 1978), and later on neutral atoms (Phillips and Metcalf, 1982; Prodan *et al.*, 1982).

In all of these "traditional" laser cooling studies, the discussion has been limited to the kinetic effects of a single frequency field on atomic motion. One consequence has been the elucidation of certain limits of force magnitude and velocity capture range. In this paper, the discussion is expanded to include the effects of multi-frequency light acting on a single atomic transition (not a repumping field). The limitations discovered for single frequency light are now substantially relaxed, resulting in immense forces and velocity capture ranges. Such huge forces enable extremely short time scales for the desired kinetic changes. Moreover, these forces are implemented by purely stimulated process - spontaneous emission (SpE) is not involved. This may have important implications for optical forces on molecules where SpE could result in their being removed from the process.

There are two kinds of optical forces in a single frequency light field, one deriving from absorption followed by SpE called the radiative force, and the other caused by absorption followed by stimulated emission called the dipole force, usually derived from the spatial dependence of the light shift (AC Stark shift, see Eq. 2). The boundary between these can be indistinct, but the nature of the optical force that arises from these two different processes is quite different. Both kinds have been amply studied and measured, and will be discussed separately below.

For nearly resonant light (at low intensity), the dominant return to the ground state following absorption is through SpE. SpE causes the state of the system to evolve from a pure state into a mixed state, and so the density matrix is needed to describe it properly. In the simplest case of the absorption of light from a laser beam, the momentum exchange between the light field and the atoms results in the radiative force $F = dp/dt = \hbar k \gamma_p$, where $k \equiv 2\pi/\lambda$ and λ is the optical wavelength, and γ_p is the excitation rate of the atoms. It depends on the laser detuning from atomic resonance $\delta \equiv \omega_\ell - \omega_a$, where ω_ℓ is the laser frequency and ω_a is the atomic resonance frequency (Metcalf and van der Straten, 1999).

At high intensity, where stimulated emission becomes important, γ_p saturates at $\gamma/2$ where $\gamma \equiv 1/\tau$ and τ is the excited state lifetime. Thus the maximum radiative force is $F_{\rm rad} \equiv \hbar k \gamma/2$. Moreover, it's convenient to define the velocity capture range $v_c \equiv \gamma/k$, limited by the Doppler shifts over the velocity range of moving atoms that takes them out of resonance. At high intensity, the absorption linewidth can be power broadened beyond γ (Metcalf and van der Straten, 1999).

For larger detuning, the momentum exchange is usually facilitated by stimulated emission. For a single plane wave there is no momentum exchange from an absorption-stimulated emission cycle, but in the presence of multiple beams, absorption from one can be followed by stimulated emission into the other. The momentum difference between these two (usually embodied in the direction of their $\vec{k}$-vectors) is imparted to the atoms, and constitutes the dipole force.

This dipole force is more easily calculated from an energy picture than from a momentum picture. It derives from the gradient of the light shift in an inhomogeneous light field such as a standing wave, and is often found by direct solution of the Schrödinger equation for a two-level atom in a single-frequency plane wave (van der Straten and Metcalf, 2016). The

solution provides the position-dependent, light-shifted dressed state energies $\hbar\Omega'$ (see Eq. 2 below).

The optical forces used for laser cooling require special properties, and these were first discussed in several references (Hänsch and Schawlow, 1975; Wineland and Dehmelt, 1975; Wineland *et al.*, 1978). The important criterion for a cooling force is a velocity dependence that is finite over some velocity range but vanishes at other velocities. Thus atoms accumulate in the region of velocity space where the force is zero or very small.

The mechanisms for the various cooling forces to vanish are completely different: in beam slowing, the Doppler and Zeeman shifts combine to cause the atoms to drop out of resonance (Phillips and Metcalf, 1982); in optical molasses, the two opposing forces just balance to make zero net force on stationary atoms (Chu *et al.*, 1985); in polarization gradient cooling, the width of the atomic wave packet exceeds the optical wavelength within the standing waves for velocities below the recoil velocity $\hbar k/M$ (Dalibard and Cohen-Tannoudji, 1989); and with the bichromatic force, there are non-adiabatic processes that cause the average force to vanish (Corder *et al.*, 2015a,b; Yatsenko and Metcalf, 2004). Note that none of these mechanisms arise directly from SpE processes.

For all schemes of cooling with the radiative force, both $F_{\rm rad}$ and v_c are limited by γ, which is an inherent property of the atoms being cooled. But the dipole force results from the sequence of absorption followed by stimulated emission using beams of different $\vec{k}$-vectors, so it is not limited by γ and can be $\gg F_{\rm rad}$. However, its velocity dependent part is usually limited to $\leq F_{\rm rad}$ and the velocity capture range is limited to less than $\pm v_c$.

B. Introduction to Two-Level Atoms

The discussions to follow rely on a few basic principles of quantum mechanics that are reviewed here for completeness and to establish the notation.

The possible states of a free atom are determined by the atomic Hamiltonian $\mathcal{H}_0$ whose stationary eigenfunctions ϕ_n have eigenenergies $E_n \equiv \hbar\omega_n$. Specifically, $\mathcal{H}_0\phi_n = E_n\phi_n$. Shining light on the atoms adds time-dependent terms to the Hamiltonian, denoted by $\mathcal{H}'(t)$, and the result is that the stationary eigenstates are mixed.

Then the wave function is $\Psi(t) = \sum_n c_n(t)\phi_n e^{-i\omega_n t}$, and substitution into the Schrödinger

equation, followed by some algebraic steps, results in

$$\dot{c}_j(t) = \frac{1}{i\hbar} \sum_n c_n(t) \mathcal{H}'_{jn}(t) e^{i\omega_{jn}t}, \tag{1}$$

where the matrix elements $\mathcal{H}'_{jn}(t) \equiv \langle \phi_j | \mathcal{H}'(t) | \phi_n \rangle$, and the frequency $\omega_{jn} \equiv \omega_j - \omega_n$. The usual textbook approach to Eq. 1 uses perturbation theory, an approximation of very limited utility in this modern era of laser spectroscopy. It can be avoided because the very narrow band excitation, characteristic of near-resonant laser light, can connect only two states (Rabi, 1937) so the sum can be reduced to only two terms and the resulting coupled differential equations can be solved directly (Allen and Eberly, 1987; Metcalf and van der Straten, 1999; van der Straten and Metcalf, 2016).

This two-level description can be clarified by replacing the ϕ_n's by $|g\rangle$ and $|e\rangle$, and by implementing the electric dipole and the rotating wave approximations. It is convenient to define the (complex) Rabi frequency that parametrises the coupling between the two states as $\Omega \equiv \langle e | e\vec{\mathcal{E}} \cdot \vec{r} | g \rangle / \hbar$. The eigenfunctions $\Psi(t)$ of a two-level atom in a monochromatic field are often described in terms of the "dressed states" of the atom (Cohen-Tannoudji *et al.*, 1977; van der Straten and Metcalf, 2016). The energy level diagram consists of the ordinary atomic energies repeated for each value of the energy of the light field, and therefore vertically displaced by $\hbar\omega_\ell$, as shown schematically in Fig. 1. Attention is focused on the closely spaced pairs of atomic states coupled by the laser light, consisting of one excited state and one ground state, denoted by $|e, n-1\rangle$ and $|g, n\rangle$ respectively, and now separated by $\hbar\delta = \hbar\omega_{eg} \equiv \hbar(\omega_\ell - \omega_a)$. In the presence of the coupling interaction, both $|e, n-1\rangle$ and $|g, n\rangle$ become mixtures of both $|e\rangle$ and $|g\rangle$.

The coupling interaction splits these eigenstates further apart by the "light shift" to

$$\hbar\Omega' = \frac{\hbar}{2} \left[\delta \pm \sqrt{|\Omega|^2 + \delta^2} \right] \tag{2}$$

where Ω is the Rabi frequency for a single traveling wave beam. Combining two of them makes a standing wave with Rabi frequency 2Ω at the antinodes. The shift of each dressed state, $\hbar(\Omega' - |\delta|)/2$, is called the light shift. In a standing wave, these light shifts vary from zero at the nodes to a maximum at the antinodes. The spatial variation of these eigenenergies results in the dipole force, found from the gradient of this energy.

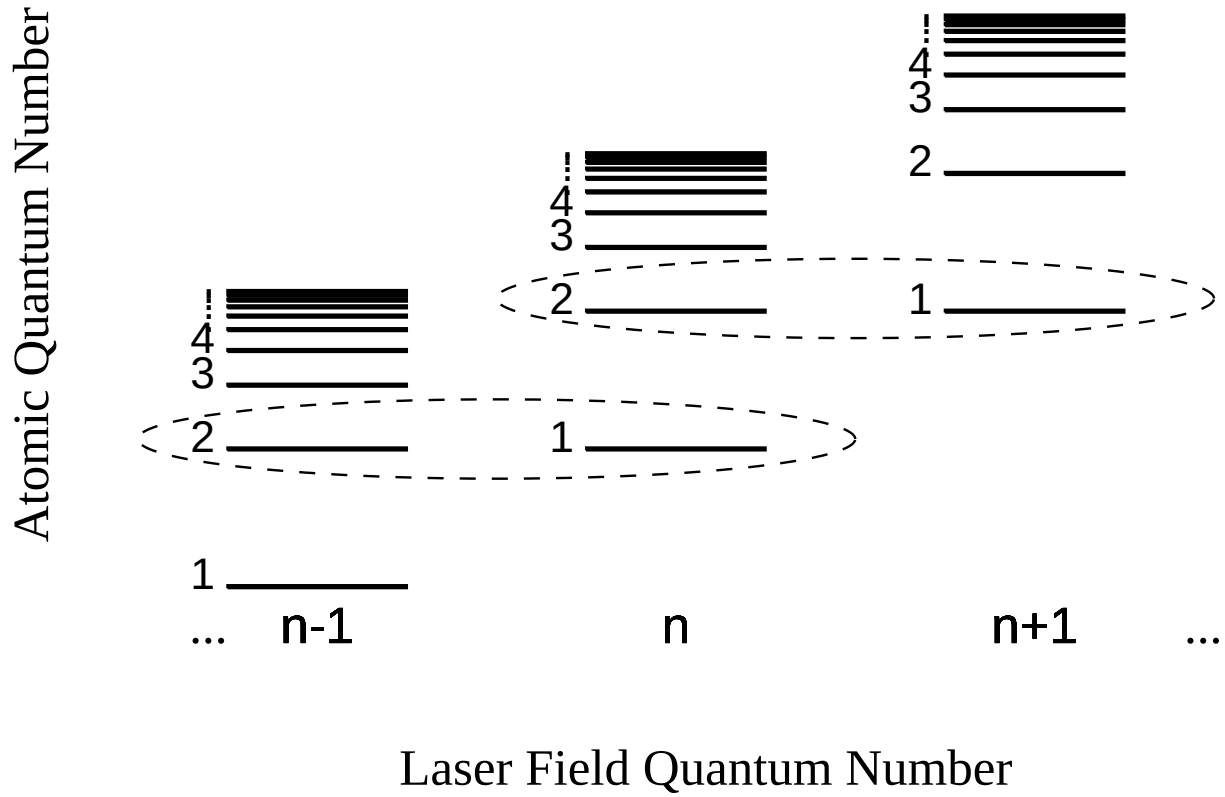

FIG. 1 Energy level diagram for the atom plus field Hamiltonian. Each vertical column has the familiar atomic level scheme, but the columns are vertically displaced by $\hbar\omega_\ell$ because of the inclusion of additional light energy of $\hbar\omega_\ell$ in each column. The nearly degenerate pairs are indicated. (Figure from (Metcalf and van der Straten, 1999).)

C. Energy and Entropy Exchange in Laser Cooling

The idea of "temperature" in laser cooling requires some careful discussion and disclaimers. In thermodynamics, temperature is carefully defined as a state variable for a closed system in thermal equilibrium with a bath. In laser cooling this is clearly not the case because a sample of atoms is always absorbing and scattering light so the system is not closed. Thermal equilibrium, of course, requires that there be thermal contact, *i.e.*, heat exchange, with the environment. Thus a system may very well be in a steady-state situation, but certainly not in thermal equilibrium, so that the assignment of a thermodynamic "temperature" is completely inappropriate. Nevertheless, it is convenient to use the label of 'temperature' to describe an atomic sample whose average kinetic energy $\langle E_k \rangle$ satisfies

$3k_BT/2 = \langle E_k \rangle$, where k_B is Boltzmann's constant.

In laser cooling, only the outgoing light can remove the thermal energy from the atomic sample. In Doppler molasses or atomic beam slowing, this is enabled because the incident light is at a frequency ω_ℓ below atomic resonance ω_a (in the laboratory frame) by $\delta < 0$. But the spontaneously emitted fluorescence has frequency $\omega_f \geq \omega_\ell$ for all emission directions in the lab frame because of the Doppler shifts, thereby mediating a net energy transfer to the light field. Thus the angular distribution of SpE mediates the energy removal via the Doppler shifts. Even in more elaborate cooling techniques such as polarization gradient cooling, $\omega_f \geq \omega_\ell$ by approximately the light shift difference between different ground state sublevels.

Moreover, SpE is further required for energy dissipation in laser cooling with single-frequency light because stimulated emission would always be at the frequency of the exciting light in both the atomic and laboratory frames, and hence preclude energy exchange. Only SpE, combined with the Doppler shift resulting from atomic motion, for example, can remove more energy than was absorbed in the excitation, thereby allowing the energy exchange required for cooling. Of course, in multi-frequency light, energy can be removed by purely stimulated processes if absorption of the lower frequency light (*i.e.* red) is followed by stimulated emission into the higher frequency field (blue).

Since laser cooling decreases the temperature of a sample of atoms, there is less disorder and therefore less entropy. The thermodynamic definition of entropy depends on thermal equilibrium. A statistical definition based on the Shannon or von Neumann formulas that involve the number of distinguishable states accessible to the system was discussed in (Metcalf, 2008) and is used herein.

In the familiar case of single-frequency light, the 4π solid angle of the SpE provides so very many states accessible to the system of [atoms+light] that it seems natural to assume that the entropy loss of the cooled atoms is also mediated by this fluorescent light. But extending this notion to the claim that SpE is therefore **required** for entropy dissipation is not necessarily correct, and some examples have been explored in (Metcalf, 2008). Thus multi-frequency light fields can enable both energy and entropy exchange with stimulated processes only.

II. TWO FREQUENCY LIGHT

A. Introduction

Optical forces have been demonstrated with single-frequency light using both radiative and dipole forces. Descriptions of these forces were originally dominated by the model of two-level atoms moving in a single-frequency laser field. The topics that could be described with this primitive model included atomic beam slowing and cooling (Phillips and Metcalf, 1982; Prodan *et al.*, 1982), optical molasses (Chu *et al.*, 1985), optical dipole traps (Chu *et al.*, 1986), optical lattices (Salomon *et al.*, 1987), band structure effects (Jessen *et al.*, 1992), and a host of others (Metcalf and van der Straten, 1999).

Soon after the earliest cooling experiments, it became clear that this simple two-level atom view was inadequate, and that the multiple level structure of real atoms was necessary to explain some experiments. Perhaps the most dramatic impact came from the discovery of cooling below the Doppler temperature $T_D \equiv \hbar\gamma/2k_B$ (Lett *et al.*, 1988). This could be explained only by polarization gradient cooling in atoms with multiple ground state sub-levels, possibly enabled by magnetic Zeeman mixing as in (Sheehy *et al.*, 1990), which is called Sisyphus cooling (Dalibard and Cohen-Tannoudji, 1989; Ungar *et al.*, 1989). In such sub-Doppler cooling of multi-level atoms, it is the dipole force, usually present in multiple beams of single-frequency light such as standing waves, that acts on the atoms. Still, the dissipation of energy and entropy is mediated by SpE, even when stimulated emission dominates.

Inclusion of the multi-level structure of atoms in the discussion provided a description of many more phenomena. In addition to the Sisyphus cooling discussed above, there is the magneto-optical trap (multiple excited state levels) and velocity selective coherent population trapping and Raman cooling (multiple ground state levels). Thus the extension from two-level to multi-level atoms gave an unexpected richness to the topic of atomic motion in optical fields. It seems natural to expect that a comparable multitude of new phenomena would be found for the motion of atoms in multi-frequency fields, but this subject has not received as much attention.

With multi-frequency light, the limitations imposed by γ have been overcome by both the bichromatic force (Cashen and Metcalf, 2001; Söding *et al.*, 1997; Yatsenko and Metcalf, 2004) and the adiabatic rapid passage force (Lu *et al.*, 2005, 2007; Miao *et al.*, 2007; Stack

et al., 2011). Such multi-frequency light can produce optical forces on neutral atoms that are significantly stronger and cover significantly larger spatial and velocity ranges than is possible with single frequency light. These capabilities arise from the use of stimulated emission to return excited atoms to their ground state. Such advantageous properties need to be described in terms of both energy and momentum exchange between the atoms and the light fields. The energy exchange derives from the frequency difference between the absorbed and emitted light, and the enhanced momentum exchange derives from the short time interval ($\ll \tau$) between the absorption and emission steps.

Excitation and stimulated emission by monochromatic light can exchange at most the tiny bit of energy associated with the atomic recoil, and this is usually balanced by the changing light shift if atoms are moving through an inhomogeneous light field (*e.g.,* a standing wave). By contrast, the use of multi-frequency light can result in absorption of one frequency and stimulated emission by another frequency (back to the original atomic state, not a Raman-like transition). Then the atomic energy change is purely kinetic, given in Sec. II.C.2 as twice the Doppler shift, and can easily be much larger than the recoil energy.

The momentum exchange between the atoms and the light cannot exceed $\pm 2\hbar k$ in a single absorption-emission cycle, but it produces this large energy exchange because $\Delta E_k \propto v$, the atomic velocity (see Sec. II.C.2 below). The force is so large because the time for these momentum exchanges is so short compared to the excited state lifetime, as in the ordinary radiative force. Thus the rapid cycling of stimulated emission enables the exchange of many times $2\hbar k$ during a single atomic lifetime τ.

B. Dipole Force Rectification

Although the non-saturable dipole force is a very attractive tool for manipulating atoms, its practical utility is limited because its sign alternates on the wavelength scale so its spatial average vanishes. The desire to extend its spatial range has produced two related proposals that exploited two-frequency fields to provide spatial rectification of the dipole force (Kazantsev and Krasnov, 1989; Voitsekhovich *et al.*, 1988). These were among the first applications of two-frequency light to optical forces.

The first attempt to extend the spatial range of the dipole force was the use of two

frequencies (driving a single transition, not a repumper). One of these methods, rectification of the dipole force, uses two standing waves of different frequencies, ω_1 and ω_2, with the light from ω_1 intense enough to provide a strong dipole force (Grimm *et al.*, 1990). Then the light shift from ω_2, with very different parameters, can be used to spatially modulate the atomic energy levels and hence the sign of the detuning of ω_1, as shown by the dotted curve in Fig. 2a. This modulation reverses the sign of the light shift caused by ω_1 with approximately the same spatial period as the dipole force, and therefore the force is rectified (Fig. 2c).

For the parameters of Fig. 2, the two standing waves maintain their spatial phase relation within $\pi/20$ over many thousands of wavelengths, much more than the $\lambda/2$ of the single frequency dipole force. This scheme was subsequently demonstrated (Grimm *et al.*, 1990; Grove *et al.*, 1995; Gupta *et al.*, 1993; Voitsekhovich *et al.*, 1989). However, ω_1 and ω_2 have to be fairly well specified, and therefore the rectification mechanism can tolerate only small Doppler shifts, putting rather severe limits on the velocity range of this rectified force (Grimm *et al.*, 1990; Grove *et al.*, 1995; Gupta *et al.*, 1993; Voitsekhovich *et al.*, 1989).

C. The Bichromatic Force

1. Origin of the Force

A second way to extend the spatial range of the dipole force uses an optical field having two beams of equal intensities and large detunings (relative to γ). This bichromatic force (BF) also provides a force much stronger than $F_{\rm rad}$ as well as a velocity range much wider than $\pm v_c$ of $F_{\rm rad}$ (Söding *et al.*, 1997). The discussion here is limited to the special case of a two-level system and two frequencies of light. Moreover, there has been important work on multi-level systems (molecules) (Aldrich *et al.*, 2016; Chieda and Eyler, 2011; Jayich *et al.*, 2014), as well as on the use of four frequencies (Galica *et al.*, 2013). Another important case is the use of two frequencies on a two-level system, but with two stages of deceleration in tandem (Chieda and Eyler, 2011). Still another application is the use of four sequential stages for atomic beam collimation (Partlow *et al.*, 2004).

The BF to be discussed here is implemented with two overlapped standing waves equally detuned from atomic resonance by $\pm\delta$, with $|\delta| \gg \gamma$ (see Fig. 3). Even in this simplest case of multi-frequency light, the bottleneck imposed on $F_{\rm rad}$ and v_c by γ can be overcome

because it produces coherent control of the momentum exchange between the light field and the atoms. The magnitude of the BF, $F_B = 2\hbar k\delta/\pi$ for the optimum value of Ω, depends on the experimentor's choice of δ, Ω, and the spatial phase difference of the standing waves, and not by atomic properties (see Eq. 4) (Söding *et al.*, 1997; Yatsenko and Metcalf, 2004). It has been demonstrated in Na (Nölle *et al.*, 1996; Voitsekhovich *et al.*, 1989), Cs (Söding *et al.*, 1997), Rb (Liebisch *et al.*, 2012; Williams *et al.*, 1999, 2000), and He (Cashen and Metcalf, 2001, 2003).

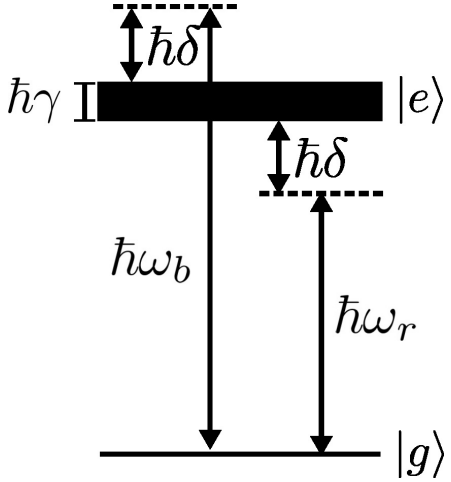

FIG. 3: Detuning scheme for the bichromatic force. The thickness of the line labeled $|e\rangle$ represents the natural width of the excited state γ, and $|\delta| \gg \gamma$ as shown.

A very useful view of the BF was given in (Grimm *et al.*, 1994, 1996), and it is instructive to examine the BF in this modified dressed atom picture because the light intensity is in the appropriate domain. In single frequency light, the dressed states pairs (without light shifts) are split by $\hbar\delta$ as a result of the Rabi oscillations between the ground and excited states ($|g, n\rangle$, $|e, n-1\rangle$), as shown in Fig's. 1 and 4a. However, the presence of the two frequencies changes each pair of the familiar multiple doublets of dressed state eigenvalues to a huge manifold of states separated by $\hbar\delta$, first described by (Grimm *et al.*, 1994) and extended by (Yatsenko and Metcalf, 2004) (see Fig. 4b).

Figure 4 shows how each component of a dressed state pair, formerly denoted by just a single field quantum number $|g, n\rangle$ or $|e, n-1\rangle$, now requires two field quantum numbers, hence $|g, b, r\rangle$ where b and r are "blue" and "red". Since the atoms that were excited by one frequency can be returned to the ground state by stimulated emission from the other frequency, thereby exchanging red light for blue (or vice versa), the result is in a new energy state for the [atom + light] system. For example, if $|g, b, r\rangle$ is excited by red light to $|e, b, r-1\rangle$, it can be returned to the ground state $|g, b+1, r-1\rangle$ by blue light as well as to $|g, b, r\rangle$ by red light. Multiple such events produce a ladder of states from just a single pair

of dressed states in single-frequency light as shown in Fig. 4b.

Each of the basis states in the ladder of Fig. 4b is connected to its two neighbors by off-diagonal matrix elements $\Omega_b(z)$ or $\Omega_r(z)$ of the standing waves. The result is the Hamiltonian matrix of Eq. 3 (truncated to 7×7).

$$\mathcal{H} = \hbar \times \begin{bmatrix} 3\delta & \Omega_r(z) & 0 & 0 & 0 & 0 & 0 \\ \Omega_r(z) & 2\delta & \Omega_b(z) & 0 & 0 & 0 & 0 \\ 0 & \Omega_b(z) & \delta & \Omega_r(z) & 0 & 0 & 0 \\ 0 & 0 & \Omega_r(z) & 0 & \Omega_b(z) & 0 & 0 \\ 0 & 0 & 0 & \Omega_b(z) & -\delta & \Omega_r(z) & 0 \\ 0 & 0 & 0 & 0 & \Omega_r(z) & -2\delta & \Omega_b(z) \\ 0 & 0 & 0 & 0 & 0 & \Omega_b(z) & -3\delta \end{bmatrix}. \tag{3}$$

Diagonalizing this Hamiltonian matrix (expanded to 30×30) produces the oscillating eigenvalues of Fig. 5. These are periodic on the scale of $\lambda/2$ because of the standing waves whose fields vary in space as shown at the bottom of Fig. 5.

Moreover, the interference of the two standing wave fields imposes a different periodicity on the scale of $\pi c/\delta$. With $\delta \sim 10^8$ s^{-1}, this is typically $\sim$1 m and is very much larger than the cm scale of most experiments. Therefore the spatial phase offset of the standing waves is considered as a fixed experimental parameter, and constitutes a spatial extension of the order of 1 m. In Fig. 5 the standing wave spatial offset is fixed at $\lambda/8$.

In this model, the BF arises from transitions of moving atoms among these manifolds at the crossings between eigenstates that are indicated by the small circles labeled "A". These are exact crossings because they occur between states coupled by one field at the nodal points of the other field (see vertical lines in Fig. 5). Thus moving atoms follow the path indicated by the heavy curved arrow of Fig. 5, so that the average BF is

$$F_B = -\frac{\langle \Delta E \rangle}{\Delta z} = \frac{2\hbar\delta}{\lambda/2} = \frac{2\hbar k\delta}{\pi}, \tag{4}$$

and for $|\delta| \gg \gamma,\ F_B \gg F_{\rm rad}$.

To assure the desired exact crossings at the points labeled "A" in Fig. 5, there are two constraints. One is vanishing of coupling to other states, and the other is that the light

shifts must cause the dressed state eigenvalues to just meet as shown. These conditions are connected via the relative spatial phase of the standing waves as discussed in (Yatsenko and Metcalf, 2004).

For our choice of this spatial phase = $\lambda/8$ (see Fig. 5), the Rabi frequencies at the standing wave antinodes must satisfy $\Omega = \sqrt{3/2}\,\delta$. This result is readily derived from the expression for Ω' of Eq. 2 (Hua *et al.*, 2016). At the points marked "A" in Fig. 5 where there are nodes in one field, the other field has strength $\Omega/\sqrt{2}$. But there are two fields that add, so the Ω term under the radical in Eq. 2 should become $2|\Omega|^2$. For the eigenvalues of two manifolds to just touch, the dressed state energy $\hbar\Omega'$ of Eq. 2 needs to be $\hbar\delta$, which yields $\Omega = \sqrt{3/2}\,|\delta|$.

2. Velocity Dependence of the Bichromatic Force

As discussed in Sec. I.A, the force needed for cooling is required to be velocity dependent, and unlike many other optical cooling forces, the BF does not vanish for atoms at rest. The BF always eventually increases atomic speeds, and when these speeds approach $v = v_B \equiv \delta/2k$, the magnitude of the force diminishes because of Landau-Zener transitions between the atomic dressed states (Yatsenko and Metcalf, 2004). These occur near anticrossings of the type indicated by the vertical ellipse labeled "B" in Fig. 5, and thereafter the atomic speeds remain approximately constant because these transitions repeat multiple times, reversing the force each time. Thus the final velocity distribution will be peaked near v_B and be narrow enough to constitute cooling. Note that both F_B and v_B scale with the value of δ.

This "speed limit" can be understood classically by considering that the momentum exchange caused by exchanging red and blue light between oppositely traveling beams is $\Delta p = \pm 2\hbar k$. For $v \gg v_r \equiv \hbar k/M$, the kinetic energy change is $\Delta E_k = Mv\Delta v = 2\hbar k v$. Since the maximum available energy for this exchange is $\hbar\delta$, v is necessarily $\leq \delta/2k$. For slower atoms, the process can occur in regions where the eigen-energies are closer together than $\hbar\delta$, and these are plentiful as shown in Fig. 5. Thus the atoms and light field can exchange energy, some of which is kinetic, and the difference is carried away by the light.

Atoms halfway to this speed limit are traveling at $v_B/2 = \delta/4k$. They traverse the regions in Fig. 5 where the loci of the eigenfunctions are approximately horizontal in a time

$t_t = d/v = (\lambda/8)(4k/\delta)$, and spend about half their time in such regions. For $\Omega = \sqrt{3/2}\,|\delta|$ this means Ωt_t = a few, providing ample time for transitions that exchange red light for blue, or vice versa, even with Doppler shifts as large as $\delta/4$.

Since the BF covers a range of velocities $v_B \gg v_c$, Doppler compensation using a multi-kilowatt Zeeman tuning magnet for example, is rendered unnecessary for slowing a thermal beam. Thus the BF is a superb method for fast, short-distance, deceleration of thermal atoms that minimizes atom loss, thereby making it a most useful and important tool.

Atoms initially within the velocity capture range $\pm v_B$ experience an approximately constant force F_B, as is evident by following the trajectories of Fig. 5. They will be accelerated to $\pm v_B$ in a characteristic "cooling time"

$$t_c = \frac{\Delta p}{F} = \frac{2Mv_B}{F_B} = \frac{\pi}{4\,\omega_r} \tag{5}$$

where $\omega_r \equiv \hbar k^2/2M = Mv_r^2/(2\hbar)$ is the recoil frequency. (Surprisingly, the cooling time for all known optical cooling schemes is not related to τ, but depends only on ω_r (Metcalf, 2008).) Even though the atoms have been accelerated to $\pm v_B \neq 0$, there is still cooling because the final temperature is determined by the width of the velocity distribution. If this distribution has been narrowed around v_B, then the atomic sample has been cooled.

A careful simulation of the BF based on the optical Bloch equations (see below) has elucidated many of its features (Hua *et al.*, 2016). It uses a spread of initial velocities and positions, and shows the temporal evolution of the velocity distribution under the influence of the BF. The strong cooling capability is shown in Fig. 6.

D. Polychromatic Forces

The extension of the BF to include more frequencies was studied numerically in (Galica *et al.*, 2013). The paper begins with a careful examination elucidating new information about the BF in the case where the beam intensities are unequal, but then goes on to consider adding frequencies detuned at various harmonics of δ to produce a polychromatic light field.

The outcomes of these studies are surprising. The parameters that produced the strongest force used equal light intensities of $\Omega = \delta$ in the first and third harmonics, thus making four

frequencies $\omega_\ell = \omega_a \pm \delta$ and $\omega_a \pm 3\delta$, (where $\delta \equiv \omega_\ell - \omega_a$). Also, they found an optimum phase offset of $\lambda/12$ in the presence of these frequencies instead of the $\lambda/8$ that produced the optimum BF.

Optimum parameter choices showed that the magnitude of the four frequency force is increased by nearly 50% over that of the BF, its velocity range is increased by nearly a factor of 3, and its average excited-state fraction is reduced from 41% to 24% (important for molecules, see Sec. V.D). Moreover, the total laser power for this four-frequency scheme is larger by only a factor of 4/3, but would have required a factor of 9 to reach this velocity range with the BF at detuning $\pm 3\delta$. Finally, the imbalanced beam intensity study suggested that the four-color force is more robust than the BF.

III. SWEPT FREQUENCY LIGHT

A. Introduction

The original model for the BF was based on the idea of π-pulses (Galica *et al.*, 2013; Söding *et al.*, 1997; Voitsekhovich *et al.*, 1988) but it has its shortcomings (see Sec. IV.C). Inverting the population of a two level system with alternate, counterpropagating π-pulses can exchange momentum between the atoms and the light field much more rapidly than the limitation imposed by γ. Even for very short pulses that don't overlap (Goepfert *et al.*, 1997; Nölle *et al.*, 1996), the fidelity of inversion by π-pulses is very limited since their effectiveness is dependent on the pulse "area" being quite precise (Allen and Eberly, 1987).

But this intuitive description led to a different idea for producing strong optical forces that arises because π-pulses are not the only way to invert the population of a two-level system. A technique called adiabatic rapid passage (ARP) was developed by the magnetic resonance community in the 1930's to do this, and it has been widely exploited since then. It is very much more robust against variations in experimental parameters such as frequency and intensity, and its application is not restricted to any region of the electromagnetic spectrum (*e.g.,* Ref's. (Hulet and Kleppner, 1983; Rubbmark *et al.*, 1981)). Its application to optical frequencies was first reported in (Loy, 1974), and it has since been used to produce very large optical forces on atoms because of its rapid momentum exchange capability (Lu *et al.*, 2005, 2007; Miao *et al.*, 2007; Stack *et al.*, 2011).

ARP is particularly well described using parameters computed from the density matrix elements in accordance with standard methods given in Ref's. (Allen and Eberly, 1987; Feynman *et al.*, 1957; Metcalf and van der Straten, 1999; van der Straten and Metcalf, 2016). Solving the Schrödinger equation with a Hamiltonian that includes the interaction between a two-level atom and the light field, along with the dipole and rotating wave approximations, produces eigenfunctions that can be written in terms of three real numbers, usually designated by u, v, and w. The light field is also represented by three real numbers, the real and imaginary parts of the Rabi frequency Ω_r and Ω_i, and the detuning δ (a complex Rabi frequency simply allows for a phase).

Then the system dynamics can be described in terms of two artificial vectors, the time-dependent Bloch vector $\vec{R} \equiv (u, v, w)$ that represents the atomic state, and the "torque vector" $\vec{\Omega} \equiv (\Omega_r, \Omega_i, \delta)$ that describes the light field. With these substitutions, the time-dependent Schrödinger equation becomes (Feynman *et al.*, 1957)

$$\frac{d\vec{R}}{dt} = \vec{\Omega} \times \vec{R}. \tag{6}$$

Under the influence of the light field, the Bloch vector $\vec{R}$ precesses about the torque vector $\vec{\Omega}$ with constant magnitude, so it can be represented as moving on the "Bloch sphere", whose two sets of overlapping coordinates are the atomic and the optical.

The representation of $\vec{R}$ on the Bloch sphere has the atomic ground state at the south pole ($w = -1$), the excited state at the north pole ($w = +1$), and superposition states anywhere else, with their phase represented by the longitude. For the representation of $\vec{\Omega}$, strongly detuned light ($|\delta| \gg \Omega$) is directed through the poles and $\delta = 0$ light is in the equatorial plane. The relative phase of $\vec{\Omega}$ is represented by the longitude on the sphere, and is relevant when there are multiple light sources. With δ and Ω both nonzero, the torque vector $\vec{\Omega}$ points elsewhere. Although the magnitude of $\vec{R}$ is necessarily unity, the magnitude of the torque vector is $|\vec{\Omega}| \equiv \sqrt{\Omega_r^2 + \Omega_i^2 + \delta^2} \equiv \sqrt{\Omega^2 + \delta^2}$, where Ω is the Rabi frequency. (Note the similarity to Eq. 2.) If the light is pulsed or frequency swept, the components of $\vec{\Omega}$ become time-dependent, thus $\vec{\Omega} \to \vec{\Omega}(t)$.

B. The ARP Process

The Bloch vector (geometric) description of the eigenfunctions allows a particularly graphical interpretation of ARP. The process consists of sweeping the optical frequency from one side of resonance to the other, so that the torque vector $\vec{\Omega}(t)$ starts and ends nearly along the polar axis, but sweeps through the equatorial plane at $\delta(t) = 0$. The process is more efficient if the start and end points of $\vec{\Omega}(t)$ are closer to the polar axis, suggesting that the light intensity should be modulated synchronously to be minimum at the extrema of the frequency sweep (*i.e.*, pulsed).

At the beginning of the frequency sweep, where the initial detuning $\delta(t = 0) \equiv \delta_0$ is much larger than $\Omega(t = 0)$, $\vec{R}$ executes small, rapid orbits near the south pole (atom in the ground state). Then, as $\delta(t)$ approaches zero and $\Omega(t)$ reaches its maximum of Ω_0, the axis of these orbits slowly drifts up toward the equator. The sweep continues toward the opposite detuning so that near the end of the sweep, where again $\delta(t) \gg \Omega(t)$, $\vec{R}$ executes small, rapid orbits near the north pole, and is finally left at the north pole (the atom is in the excited state). The direction of the frequency sweep, namely the sign of $\dot{\delta}(t)$, is of no consequence (see Eq. 6) as long as $\vec{\Omega}(t)$ is essentially polar at the ends of the sweep.

There are certain traditional constraints for this process to occur efficiently. First, $|\vec{\Omega}(t)|$ must be large enough so that $\vec{R}$ makes very many precessions about $\vec{\Omega}(t)$ during the sweep time given by π/ω_m, where ω_m is the sweep rate. This means that $|\vec{\Omega}(t)| \gg \omega_m$. For a uniform frequency sweep, $\dot{\delta} = \delta_0\omega_m/\pi$, where $\pm\delta_0$ is the sweep range. This "adiabatic following" of $\vec{\Omega}(t)$ by $\vec{R}$ produces the "A" in ARP.

Second, the entire sweep must occur in a time short compared to the atomic excited state lifetime to minimize the effects of SpE during the sweep, and thereby preserve coherence between the atom and the radiation field. This requires $\omega_m \gg \gamma$, or $\dot{\delta} \gg \delta_0\gamma/\pi$, and constitutes the "rapid" condition in the name ARP. These are two conditions on the sweep rate and on $|\vec{\Omega}(t)|$ that must be met independently, in addition to their combination $|\vec{\Omega}(t)| \gg \gamma$. Of course, when $\delta(t)$ is very small, this condition applies to $\Omega(t)$

Finally, it is required that $\delta_0 \gg \Omega(t)$ at the extrema of the sweep so that the torque vector $\vec{\Omega}(t)$ is nearly polar at those points. This is readily achieved by pulsing the light intensity. Thus δ_0 and Ω_0 are the highest frequencies in the system. All these conditions

can be written together as

$$\delta_0 \sim \Omega_0 \gg \omega_m \gg \gamma. \tag{7}$$

The timing scheme for ARP-based absorption-stimulated emission cycles is illustrated in Fig. 7. A pulse of duration π/ω_m from one direction (*e.g.,* from the left) is represented by the half-period sine wave in the upper trace, and its upward frequency sweep is represented by the curve in the lower trace. A second pulse, incident from the opposite direction (*e.g.,* from the right), is represented by the second half-period sine wave, also with an upward frequency sweep. Then there is a dead time of $2\pi/\omega_m$ for experimental reasons discussed below (Miao *et al.*, 2007). The sweeps of δ are both shown as from negative to positive values, but this is not required, and sequential pulses can also be swept in opposite directions, thus producing a sine-wave frequency modulation.

The trajectories of both $\vec{\Omega}(t)$ and $\vec{R}$ are shown in Fig. 8a. Here $\vec{\Omega}(t)$ sweeps in a smooth arc from pole to pole (red curve), and $\vec{R}$ orbits closely around $\vec{\Omega}(t)$ as it adiabatically follows (black curve). Under these conditions $\vec{R}$ is efficiently moved from one pole to the other, meaning that the population is inverted. A concomitant effect is the exchange of momentum $\hbar k$ between the atom and the light field. Unlike the π-pulse method, this process is very robust against optical frequency and amplitude variations, as well as the values of δ_0 and Ω_0. If the sweep is too fast, or if there are other violations of Eq. 7, the final position of $\vec{R}$ at the end of the swept pulse may not be at the opposite pole, thus compromising the adiabaticity of the process.

Figure 8b shows an orbit that is nearly as robust as that of Fig. 8a, but with parameters that are well outside those of Eq. 7. Unlike the case for Fig. 8a, $\vec{R}$ and $\vec{\Omega}(t)$ are nearly orthogonal when they pass through the equatorial plane. The sweep of Fig. 8(b) is also adiabatic, although in a different sense, and is more suitable as a source for optical forces because it allows much faster absorption-stimulated emission cycles. This prediction from (Lu *et al.*, 2005) has been experimentally corroborated (Miao *et al.*, 2007).

A simple model calculation of the magnitude of the ARP force begins by considering that the momentum transfer in one half-cycle (two pulses) of ω_m is $2\hbar k$. First, a frequency-swept laser beam from one direction excites the atoms and transfers $\hbar k$, and then another beam from the opposite direction and whose sweep is delayed, drives them back to the ground state and also transfers $\hbar k$. Since the time for two swept pulses is $2\pi/\omega_m$, the force is

$F_{ARP} \equiv 2\hbar k/(2\pi/\omega_m) = \hbar k\omega_m/\pi$.

However, to reduce the deleterious effects of SpE, there is an experimentally inserted delay time with no light of $2\pi/\omega_m$ following each pulse pair, and thus the total time is $4\pi/\omega_m$, as shown in Fig. 7. This reduces the average force in this model to $F_{ARP}/2 = \hbar k\omega_m/2\pi$. Since ω_m can easily be many times γ, this force readily exceeds $F_{\rm rad}$.

In the course of modeling ARP, care must be taken to consider the phase of the light fields. One consideration derives from the fact that ω_m and the swept optical frequency are not commensurate so that Ω_r/Ω_i is different for each pair of pulses ($\phi_{\rm pp}$ in Fig. 7). This can change the trajectory of $\vec{R}$ on the subsequent pulse. Also, if two different lasers are used to produce the pulses from left and right in Fig. 7, then their relative phase $\phi_{\rm rel}$ can also cause trajectory changes.

C. A Dressed Atom Description of ARP

The familiar dressed atom description of a two-level atom in a nearly resonant light field provides another insight into the ARP process. In Fig. 4a the light frequency ω_ℓ is below the atomic resonance frequency ω_a so that absorption into $|e, n-1\rangle$ results in a higher energy of the [atom + laser] system. By contrast, for $\omega_\ell > \omega_a$ the state $|e, n-1\rangle$ would lie below the state $|g, n\rangle$. Thus the energy ordering of the dressed states in a single frequency light field reverses with the sign of δ.

Now consider the plot of Eq. 2 shown in Fig. 9. At the boundary plane where $\Omega(t) = 0$, the state $|g, n\rangle$ lies above (below) $|e, n-1\rangle$ for $\delta > 0$ ($\delta < 0$) as discussed above. For $\Omega(t) \neq 0$ the wavefunctions are mixtures, forming the familiar dressed states. The ARP pulses cause atoms to follow a trajectory such as indicated by the heavy arrow: a sweep from one extreme of δ to the opposite extreme that doesn't change energy sheets inverts the atomic system. In the case of Fig. 9, the sweep begins on the upper sheet with $\delta(t) = +\delta_0$ and the atom in the ground state. It goes through resonance and on to $\delta(t) = -\delta_0$ and the atom ends up in the excited state.

Even for the case of frequency-swept cw light, as long as $\delta_0 \gg \Omega(t)$, the path followed in Fig. 9 is a straight line parallel to the $\Omega = 0$ plane, and the atomic energy levels go through an anticrossing. If the sweep is slow enough, the energy sheet is not changed, and ARP still

occurs. Faster sweeps could allow Landau-Zener (LZ) transitions between sheets and ARP fails (see (Rubbmark *et al.*, 1981)).

Making a significant change of atomic velocities would require very many such repetitive sweeps that each exchange momentum $\hbar k$, and so the probability for non-adiabatic transitions must be kept very small for this to be successful. The probability of such unwanted LZ transitions can be found from the small fraction of population on the "wrong" energy sheet at the end of each sweep where $\Omega = 0$ and the eigenstates are exactly the bare states.

The probability of such LZ transitions can become minuscule if the path maintains a constant separation between the sheets. In one case of such a "circular sweep", the time-dependence of the Rabi frequency can be described by $\Omega(t) = \Omega_0 \sin \omega_m t$ and the frequency sweep by $\delta(t) = \delta_0 \cos \omega_m t$. The special case of $\Omega_0 = \delta_0$ has been studied in some detail (Sawicki and Eberly, 1999). The consequence of this special case is that $\vec{\Omega}(t)$ satisfies

$$\frac{d\vec{\Omega}(t)}{dt} = \vec{A} \times \vec{\Omega}(t) \tag{8}$$

where $\vec{A}$ is an artificial constant vector so that $|\vec{\Omega}(t)| = \sqrt{|\Omega(t)|^2 + \delta(t)^2}$ is constant. If the LZ formula were used here, the probability of the non-adiabatic transition $P_{NA} = e^{-\pi\eta/2}$ would vanish because $d|\vec{\Omega}(t)|/dt = 0$ ($\eta \equiv |\vec{\Omega}(t)|^2/(d|\vec{\Omega}(t)|/dt)$). This expression for P_{NA} is asymptotically correct for large δ_0 ($\delta_0 \gg \omega_m$), but the variations of P_{NA} as obtained in (Sawicki and Eberly, 1999) are lost.

D. An Alternative Model for ARP

A different view of ARP arises from considering the pulse pairs. If each pulse produces an approximate inversion of the Bloch vector $\vec{R}$, then a successive pair applied to a ground state atom returns it to the region of the south pole of the Bloch sphere. This can be viewed as a small rotation of the Bloch sphere instead of a rotation of the Bloch vector. If each pulse pair returned $\vec{R}$ precisely to the south pole, the rotation axis would be polar. For the non-ideal case, the axis is not polar and the rotation is finite, so $\vec{R}$ is slightly displaced from the pole. A subsequent pulse pair would repeat the same rotation, and the locus of end points of $\vec{R}$ would be a small circle near the south pole, as shown in Fig. 10.

This view is especially helpful for understanding the case of non-ideal pulses, or the effect of a very large number of pulses. For a small number or for nearly ideal pulses,

the trajectories are confined to a narrow band as shown in Fig. 4 of (Lu *et al.*, 2005). Deviations from this results in displacements of $\vec{R}$ to distant places on the sphere, and a resulting weakening of the ARP force.

IV. PULSED LIGHT

A. Introduction

Any kind of pulsed light is necessarily composed of multiple frequencies, so optical forces deriving from such light can be viewed as consequences of the non-monochromatic spectrum. These pulses can have a simple shape resulting in a symmetric spectrum, or a more complicated shape with an almost arbitrary spectrum. The center frequency of the pulse can be varied between sequential pulses, or even during the pulse (see Sec's. III and IV.D above). With both pulse envelope and spectrum available as additional degrees of freedom, there is an immense range of variations.

B. Forces and Traps From Simple Pulses

The earliest discussion of optical forces produced by pulsed light was by (Kazantzev, 1974). The force depends upon the position-dependent arrival time (or relative optical phase) of pulses in counterpropagating light beams. It is necessary for each of the pulses to be short compared to their repetition times so that their positions are well-defined. Also, they need to contain enough energy to be approximately π-pulses so that the atomic transitions induced by them have high probability.

This idea was first experimentally tested by (Voitsekhovich *et al.*, 1989) where an atomic beam was deflected by directing it through the intra-cavity beam of a laser to enable sufficiently high intensity. The laser was oscillating on two modes, and the phase difference between them depended on the distance from the atoms to the cavity mirror. Although the deflection, and consequently the force, was not large, it was clearly larger than $F_{\rm rad}$ so it unequivocally demonstrated that Kazantzev's idea was correct.

The idea was further tested in the mid 1990's by two more experimental demonstrations using ps pulse trains from mode-locked lasers (Goepfert *et al.*, 1997; Nölle *et al.*, 1996).

In both of these cases, the authors deflected and/or focused an atomic beam, and were indeed able to demonstrate a force that was $\gg F_{\rm rad}$. In a later variation, there was a study using only four discrete frequencies to produce pulses by Fourier synthesis, using appropriate harmonics of bichromatic light fields (Galica *et al.*, 2013).

The configuration of colliding pulse trains can also make an atom trap in one dimension. Let z_0 be one of the many spatial positions where the counterpropagating pulses exactly overlap. For an atom located at $z < z_0$, the pulse from the negative z side will always precede its counterpropagating partner. Then that first pulse can excite the atom, transferring momentum $+\hbar k$, and the second one can induce stimulated emission, transferring another $+\hbar k$. For an atom located at $z > z_0$, both momentum transfers are $-\hbar k$ because the pulse order reverses. Where the pulses overlap at $z = z_0$ the force vanishes because there is essentially a pulsed standing wave with no temporal bias for excitation *vs.* stimulated emission. Thus there is always a force toward z_0, hence the arrangement constitutes a trap in 1-D. As long as there is no SpE in the short interval between the pulses of a pair, the force direction is preserved.

The "focussing" described in (Goepfert *et al.*, 1997) is the result of the "1-D trap" acting for a short time as the atoms passed through the light field (not actually a static trap). (This process was re-discovered and described by (Freegarde *et al.*, 1995) and carefully analyzed by (Romanenko and Yatsenko, 2011).)

A similar situation applies for the case of the BF discussed in Sec. II.C.1. In this case, the dominant direction of the force depends on the relative spatial phase of the standing waves determined by the atom-mirror distance. The different force directions can be seen from the upward and downward sloping possible trajectories of Fig. 5, but these actually apply to different positions where one or the other dominates. Thus the system also constitutes a 1-D trap. This case was carefully analyzed in (Romanenko *et al.*, 2016), and this paper also provides a good review.

C. Π-Pulse Model of the Bichromatic Force

The early descriptions of the BF began with travelling waves carrying both frequencies, thereby comprising modulated carrier waves, as shown in Fig. 11 (Söding *et al.*, 1997).

These were retroreflected to produce counterpropagating beams of quasi-pulses with the optical carrier frequency. Their amplitudes and durations were chosen to satisfy the π-pulse criterion, resulting in the "π-pulse model" (Söding *et al.*, 1997). The time delay between incident and reflected beams was chosen so that an incident "π-pulse" would excite an atom, the counter-propagating one would de-excite it, and the process would impart momentum $2\hbar k$ in a time that could be much shorter than τ, thereby producing a force much larger than $F_{\rm rad}$. The model fell short because of the pulse overlaps, and has been replaced by the dressed atom picture of Sec. II.C.1.

D. Pulsed Light for Adiabatic Rapid Passage

The Adiabatic Rapid Passage force discussed in Sec. III above also uses pulsed light, but in a different way. The pulse is used to control the direction of the torque vector $\vec{\Omega}$ as the detuning is swept through $\delta = 0$. At either end of the frequency sweep where δ is very large, it's desirable to have $\vec{\Omega}$ be nearly polar so the magnitude of Ω should be very small or zero. Pulsing the light during the frequency sweep can accomplish this.

V. OBSERVATION AND MEASUREMENT OF OPTICAL FORCES IN MULTI-FREQUENCY LIGHT

The full potential of optical forces produced by multi-frequency light has yet to be realized in the laboratory. There was an early experiment that demonstrated the existence of a two-frequency force resulting from stimulated emission processes, but the results were limited to simply observation (Voitsekhovich *et al.*, 1989). There were also early experiments with dipole force rectification that were limited in velocity (or kinetic energy) range as discussed above (Grimm *et al.*, 1990; Grove *et al.*, 1995; Gupta *et al.*, 1993).

In experiments modeled as π-pulse sequences that rapidly exchange momentum by inverting the atomic populations using counterpropagating pulsed beams, a few groups were able to produce forces somewhat larger than $F_{\rm rad}$. In (Nölle *et al.*, 1996) the authors deflected a beam of Na and found a force as large as $6 \times F_{\rm rad}$ with 440 ps pulses separated by 1 ns. In (Goepfert *et al.*, 1997), the authors used ~ 30 ps pulses on Cs and found a force

$\approx 3 \times F_{\rm rad}$. These measurements were in good agreement with the results calculated from their model. Such short pulses have a bandwidth > 10 GHz, large enough to comprise the multiple frequencies needed to satisfy the criteria discussed above. By contrast, both the BF and the ARP force have shown much larger magnitudes and velocity capture ranges.

A. Bichromatic Force Experiments on Alkali Atoms

Apart from early demonstrations discussed above (Voitsekhovich *et al.*, 1989), the first use of the BF to show a huge force and velocity capture range, as well as a large spatial extension, was reported in (Söding *et al.*, 1997). These authors aligned the counter-propagating, bichromatic laser beams with the axis of a Cs atomic beam, using an oven whose back side was transparent so the laser and atomic beams had the same axis.

The longitudinal velocimetry exploited the frequency dependence of the fluorescence from an independent, tunable probe laser via the Doppler shifts. The interaction length was limited by performing the velocity measurement only 10 cm beyond the exit aperture of the Cs oven. The measured force was $10\times$ larger than $F_{\rm rad} \equiv \hbar k\gamma/2$, as expected from their parameters, and it spanned a velocity range as large as $50\times$ that of $v_c \equiv \gamma/k$. Several careful experimental tests confirmed that the observations agreed well with the π-pulse model of the BF.

The next reported BF experiments were done in Rb, using a force transverse to an atomic beam (Williams *et al.*, 1999, 2000). With a transversely movable slit in the atomic beam to determine the angle between it and the laser beams that produced the BF, these authors were able to make a direct comparison between the observed and calculated velocity dependence of the BF. As shown in Fig. 12, the data agreed very well with numerical calculations based on the optical Bloch equations, using a program developed by (Söding *et al.*, 1997).

The π-pulse condition is readily found to be $\Omega = \pi\delta/4$ and differs by $\sim 50\%$ from the dressed state value of $\Omega = \sqrt{3/2}\,\delta \approx 1.22\,\delta$ (see Sec. II.C.2). The measurements and calculations of panel (f) of Fig. 12 nearly correspond to this π-pulse condition, and clearly show that it is not optimal. These results provide the justification for using the dressed atom description of the BF. Panel (a) of Fig. 12 corresponds to $\Omega = 1.19\,\delta$, just a bit below the optimal dressed state value given above.

B. Bichromatic Force Experiments on Helium

The large magnitude of the BF that derives from its rapid momentum exchange rate makes it especially suitable for atoms lacking an easily accessible, excited state with a short lifetime. Alkali atoms are readily slowed and trapped in a small cell directly from a thermal vapor, but the slowing length for He using $F_{\rm rad}$ is $\sim$ 2 m. Thus the BF seems especially well-suited for manipulating He atoms.

The first BF experiments on the metastable 2^3S state of He (He*) reported observation of a beam-deflecting force $\approx 11 \times F_{\rm rad}$ and a slowing force $\approx 10 \times F_{\rm rad}$ that reduced the atomic velocities by $\sim$ 100 m/s $\approx 1100 \times \gamma/k$ (Cashen and Metcalf, 2001). This was only $\approx 2/5$ of the expected force based on the 45 γ detuning that was used, but many experimental aspects were not optimized. These experiments were made possible by the technological advances in optical amplitude and frequency modulation by the telecom industry that could be exploited for driving the transition $2^3S_1 \rightarrow 2^3P_{1,2,3}$ of He* at $\lambda = 1083$ nm.

A subsequent paper reported 2-D collimation of a beam of He* with four separate stages (Partlow *et al.*, 2004), needed because the BF pushes in only a single direction (Söding *et al.*, 1997). Each of the four counterpropagating beam pairs was tuned to push left, right, up, or down resulting in full collimation of the atomic beam. The four interaction regions were each only 10 mm long, and the total collimation region spanned 50 mm along the beam direction (see Fig. 13).

During the short collimation interval, the atomic sample could expand by only $\approx 500\,\mu$m about its original size, so that its spatial extent was essentially doubled. The transverse velocity compression ratio of ~ 12 represents a phase space compression of $\sim \times\, 6$ in each dimension. This very bright beam was subsequently used for lithography (Allred *et al.*, 2010; Reeves, 2010) because the 20 eV internal energy of He* could be used to expose a resist, as shown by the pioneering work of (Petra *et al.*, 2004a,b).

1. Cooling Without Spontaneous Emission

There is a long-standing and widely-held belief in the laser cooling community that the randomness of SpE is the only way to dissipate the entropy lost by a vapor of atoms undergoing laser cooling. Reference (Metcalf, 2008) has shown that SpE is not the only way of removing the entropy, and that the laser fields themselves may be capable of absorbing

it. There are many different kinds of entropy sinks when ground state atoms (pure state) interact with multiple incoming laser beams (pure states) to form a mixed state, even with purely stimulated processes (Metcalf, 2008). However, this notion requires that the light field be included as part of the system, and not just as an external potential.

Reference (Metcalf, 2008) began by showing that energy conservation in ordinary laser cooling requires that both the fluorescent light field and the laser light field be considered as part of the system. It argued that doing so provided for energy conservation between the light and both the atomic internal energy and its kinetic motion, as well as preservation of unitarity of the system. Furthermore, it claimed that the entropy loss, usually dismissed with vague references to SpE, can be described as merely an exchange between different parts of the system so it does not violate the Liouville theorem. The system entropy is lost when the light goes out and hits the walls, and these are not part of the system.

A subsequent paper described experiments designed to test this concept that used a time comparable to the SpE cycle time, so that SpE played a negligible role (Corder *et al.*, 2015b). The authors chose the transition $2^3\mathrm{S} \leftrightarrow 3^3\mathrm{P}$ in He* at λ =389 nm, whose cooling time given in Eq. 5 is $\approx$ 380 ns, and did the experiment in $\approx$ 200 ns by restricting the atom-laser interaction time. Since $\tau \approx 106$ ns, and the time averaged excited state population is ~ 0.4 (Galica *et al.*, 2013), the average SpE cycle time is $\approx$ 260 ns.

The experiment comprised transverse cooling of an atomic beam of He* using laser beams that crossed the atomic beam just a few mm from the source aperture. The cooling was manifest by the narrowed spatial distribution of the atoms at a detector 63 cm downstream from this interaction region. The measurements were compromised by geometrical effects, largely caused by the longitudinal velocity distribution of the atomic beam that was centered at $\approx$ 1000 m/s but had a FWHM of $\approx$ 400 m/s. This 400 m/s range caused those atoms with a given transverse velocity to be spread out at the detector by a distance corresponding to a few m/s.

The data in Fig. 14 were taken with $\delta = 2\pi \times 25$ MHz, chosen because of intensity and power considerations, and corresponding to a capture range $v_B \approx \pm 4.9$ m/s. There is a hole where atoms are moved from the -6 to +2 m/s range, consistent with $2v_B$, and a bump where they accumulate in the +2 to +11 m/s range, while those initially between 2 and 11 m/s remain. (The initial zero of velocity is apparently at -2 m/s.) The small bump near $v = -7$

m/s arises because a small fraction of the atoms enter the light field at a point in space and a time when the force is actually in the opposite direction, and is well understood. Thus the initial velocity range of interest, $\Delta v_i \approx 17$ m/s, was reduced by $\times 2$ to Δv_f as shown in Fig. 14 (see Sec. II.C.2), thereby reducing the temperature by $\times 4$. In addition, the experiment showed a net compression of occupied phase space volume because the spatial expansion of the atomic sample was limited by the short interaction time to $\sim 5\lambda$ and the original sample size was 500 μm $> 10^3\lambda$.

In spite of the geometrical limitations, the results shown are unequivocal. The separation between the bump and the hole in Fig. 14 is ~ 9 m/s $\approx 35 v_r$, thereby eliminating the radiative force from consideration. The experiments clearly demonstrated that cooling and phase space compression of an atomic sample can be accomplished without SpE by using a two-frequency laser field to accommodate energy and entropy removal.

The BF is the simplest extension from single-frequency forces, although there have been studies of other forces from polychromatic fields (Galica *et al.*, 2013; Stack *et al.*, 2011) that also derive from purely stimulated processes. Also, their velocity dependence that enables cooling does **not** derive from SpE. Because multifrequency light can produce cooling without SpE, there is enormous interest for many applications, including ultra-fast or ultra-compact cooling and direct cooling of molecules.

2. Multi-Frequency Force

At first sight, the description of the BF in Sec. II.C.2 suggests that the velocity capture range of $v_B = \pm\delta/2k$ is limited by only the accessible values of δ. The limitation arises because of its relation with the optimum value of $\Omega = \sqrt{3/2}\,\delta$, and the needed light intensity therefore scales with δ^2. Thus a wide velocity capture range for fast atoms such as He* requires high optical power. This and other limits to the velocity capture range have been carefully considered by (Chieda and Eyler, 2012). For example, these authors estimated the effects of phase imperfections and intensity imbalances, as well as Doppler-induced frequency shifts. These were found to have significant deleterious effects at large values of δ.

One way that (Chieda and Eyler, 2012) addressed the need for high power was by considering a two-stage, tandem pair of atomic beam slowing regions, each having smaller values

of δ and Ω. Clearly tandem deceleration stages, each using δ and hence $\Omega = \sqrt{3/2}\,\delta$, could cover a velocity range $2\delta/k$ and require two sets of beams of intensity $\propto 3\delta^2$ By contrast, a velocity capture range of $2\delta/k$ in a single region would require an intensity $\propto 6\delta^2$.

Another scheme tried in (Chieda and Eyler, 2012) to extend the velocity capture range with limited optical power was to sweep the detuning in synchrony with the atomic velocities, as the atoms were slowed by the BF. Thus the sweep could cover a large frequency range, but the capture range at any instant, and the concomitant intensity requirements, were considerably reduced. Figure 15 shows the measured slowing of a He* beam by $0.88\,\delta/k$ with the ordinary BF, but $2.84\,\delta/k$ with the center frequency swept by 300 MHz, about $4\,\delta$. The loss of atoms is readily attributed to several experimental artifacts, but the basic features of the measurements agree well with the simulation presented along with the experiments.

C. Adiabatic Rapid Passage (ARP) Experiments on Helium

In some sense, the ARP force is also a multifrequency force, just as in Sec. V.B.2 above, but it is implemented quite differently. Instead of several discrete frequencies acting on the atoms simultaneously or sequentially, a single laser field is both amplitude and frequency modulated, as described in Sec. III.B. The spectrum of the light in Fig. 16 shows that the light has multiple frequencies because it's a chirped pulse, not a pure sine wave.

The pulses are characterized by their maximum values of the Rabi frequency Ω_0 and the range of the frequency sweep $\pm\delta_0$ as shown in Fig's. 7 and 9. The ARP force has been calculated using Eq. 6 for various values of these parameters, and a force map is shown in Fig. 17a.

The ARP force was measured using a well-collimated beam of He* atoms that emerges from 0.5 mm aperture and is collimated by a vertical slit, 250 μm wide, 24 cm downstream. Carefully tuned and modulated light beams cross the atomic beam perpendicularly to drive the $2^3S_1 \rightarrow 2^3P_2$ transition at $\lambda = 1083$ nm. The atoms strike an MCP ~ 36 cm downstream whose output electrons are accelerated to a phosphor screen that is viewed by a CCD camera. The ARP force deflects the atoms, and a typical image is shown in Fig. 18. The measured force is extracted from the experimental geometry, and an experimental force map is shown

in Fig. 17b.

FIG. 18: The bright vertical line is an image of the collimating slit. The profile of the atoms deflected to the right in the indicated rectangle is analyzed to find the average deflection for plotting in Fig. 17b.

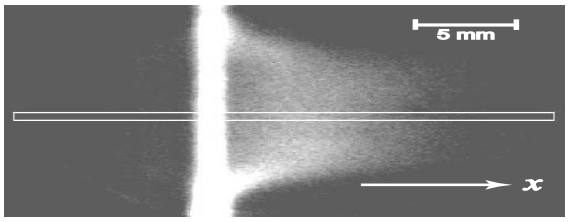

D. Studies of Multifrequency Forces in Molecules

Laser cooling of molecules has attracted considerable interest for very many years. Applications of cold molecules include, but are not limited to, tests of fundamental symmetries and forces, precision measurements, dynamics of complex systems, quantum information and memory, many-body physics, and quantum chemistry. Molecules can have many properties not found in atoms, especially their body-fixed electric dipole moments whose anisotropic interactions have been the subject of many recent studies. A few years ago there were two special journal issues with multiple discussions of such applications (Buzek *et al.*, 2004; Carr *et al.*, 2015). The lead articles in these two issues are superb reviews of the field of cold molecules (Carr *et al.*, 2009; Doyle *et al.*, 2004). More recently the field has been brought up to date in a special issue of the Wiley journal ChemPhysChem (Doyle *et al.*, 2016).

There are many ways of producing cold molecules, but laser cooling is generally not a good choice. The velocity change from a single optical absorption-emission cycle is limited to a few cm/s, and laser cooling becomes useful only by repeating such cycles about 10^4 times. This requires that the return to the ground state brings the system back to the initial sublevel so that the fixed frequency light field can cause another absorption. But unavoidable SpE into the multiplicity of vibrational and rotational sublevels of molecules precludes such cycling transitions. There have been a number of elaborate schemes to overcome such limitations to cooling molecules, *e.g.* (Bahns *et al.*, 1996; Jayich *et al.*, 2014; Shuman *et al.*, 2009; Zhelyazkova *et al.*, 2014), as well as several examples of trapping (Barry *et al.*, 2014; Marx *et al.*, 2015; Weinstein *et al.*, 1998). All of these schemes involve multiple repumping lasers and thus are indeed complicated and expensive.

On the other hand, cold molecules have been produced by photoassociation and by Fes-

hbach resonance combination of laser-cooled atomic samples (see (Fioretti *et al.*, 1998; Lett *et al.*, 1993, 1995; Miller *et al.*, 1993; Williams and Julienne, 1994) and the work of many others), by deceleration of a molecular beam (Bethlem *et al.*, 1999; Marx *et al.*, 2015), by buffer gas cooling (Doyle *et al.*, 1995; Weinstein *et al.*, 1998), by elaborate, multiple laser schemes (Bahns *et al.*, 1996; Jayich *et al.*, 2014; Shuman *et al.*, 2009; Zhelyazkova *et al.*, 2014), and by many other various protocols. (These cited articles are just a sample list and not intended to be comprehensive.) The authors of (Doyle *et al.*, 2004) wrote "There are now at least nine different techniques used to produce cold molecules, a number that increased from zero over the past eight years."

The BF seems ideally suited to optical cooling of molecules because the effects of SpE, that could populate the plethora of molecular ground state sublevels, can be much reduced. This happens because the strength of the force allows for short experimental times, thereby suppressing the effects of SpE (Corder *et al.*, 2015a,b). One of the early studies of the BF in molecules considered the simple case of CaF (Chieda and Eyler, 2011), and others have followed (Aldrich *et al.*, 2016; Hemmerling *et al.*, 2016). CaF was chosen because it has an easily accessible, quasi-cycling transition and because it has structural properties of special interest for ultra-cold molecule studies. Reference (Aldrich *et al.*, 2016) is a followup of (Chieda and Eyler, 2011), and has a particulary extended and detailed study, as well as a simulation of the BF in CaF.

The ARP force is also very well-suited for molecules, again because its strength allows a short interaction time. In (Jayich *et al.*, 2014) there is a detailed study of ARP in SrH. This was chosen because it has a strong optical transition out of the ground state that is readily accessible by a Ti:Sapphire laser and is also nearly cycling. The authors have done a careful study of the energy level structure as well as a Monte-Carlo simulation of the process.

A third example is found in (Dai *et al.*, 2015; Yang *et al.*, 2017) where the topic is BF-slowing of MgF. Like the other molecules, MgF was chosen for optical accessibility and a nearly-closed transition. Their calculations and model includes very small level splittings such as fine and hyperfine structure as well as Zeeman degeneracies. Their numerical calculations proceed by integrating the time-dependence of the density matrix for a large number of internal levels. A simplified version is also presented.

There are surely other examples but these three chosen cases are representative. They

illustrate the complexity of the problem as well as what can be done to address it. Experiments are under way in several different laboratories.

VI. SUMMARY AND CONCLUSIONS

Multi-frequency light can produce optical forces on neutral atoms that are considerably stronger and cover considerably larger spatial and velocity ranges than is possible with single frequency light. Such capabilities are enabled by using stimulated emission to return excited atoms to their ground state. The force is so large because the time for the rapid cycling produced by stimulated emission can be very short compared to the excited state lifetime. This allows the exchange of many times $2\hbar k$ during a single atomic lifetime, in contrast to the ordinary radiative force. The energy exchange of each cycle can be very large because atoms can absorb one frequency and undergo stimulated emission of a different frequency.

A wide range of successful tests of the models presented in Sec's. II, III, and IV are described in Sec. V. The models are well-corroborated qualitatively, and in many instances quantitatively as well. These include dipole force rectification, bichromatic force, multi-frequency force, cooling without SpE, adiabatic rapid passage force, application to "open" systems such as molecules, etc. These tests have been performed on many alkali atoms, He, MgF, and perhaps others.

Further applications and the full potential of multi-frequency light to produce forces on atoms and molecules have yet to be realized in the laboratory. In the case of Rb and Cs, cold, dense samples can be extracted from room temperature vapors, but for other atoms whose room-temperature vapor pressures are too low, the compact apparatus enabled by the strength of the forces seems very attractive (atoms on a chip and other configurations). Using such forces on molecules provides great appeal because the losses resulting from SpE to the multitude of ground state sublevels can be significantly reduced. There will surely be new results from experiments currently underway in many laboratories throughout the world.

I wish to thank Martin G. Cohen for many helpful suggestions.

* Supported by the O.N.R.

REFERENCES

Aldrich, L., S. E. Galica, and E. E. Eyler (2016), Phys. Rev. A **93**, 013419.

Allen, L., and J. Eberly (1987), *Optical Resonance and Two-Level Atoms* (Dover, New York).

Allred, C. S., J. Reeves, C. Corder, and H. Metcalf (2010), J. App. Phys. **107**, 033116.

Ashkin, A. (1970), Phys. Rev. Lett. **24** (4), 156.

Ashkin, A. (1978), Phys. Rev. Lett. **40** (12), 729.

Ashkin, A., and J. Gordon (1983), Opt. Lett. **8** (10), 511.

Bahns, J. T., W. C. Stwalley, and P. L. Gould (1996), The Journal of Chemical Physics **104** (24), 9689.

Barry, J. F., D. J. McCarron, E. B. Norrgard, M. H. Steinecker, and D. DeMille (2014), Nature **512** (8), 286.

Bethlem, H., G. Berden, and G. Meijer (1999), Phys. Rev. Lett. **83**, 1558.

Buzek, V., H. Kersten, and A. Solov'yov, Eds. (2004), *Special Issue on Ultra-cold Polar Molecules: Formation and Collisions* (The European Physical Journal D, **31**, November).

Carr, L., D. DeMille, R. Krems, and J. Ye, Eds. (November 2014 August 2015), *Focus on New Frontiers of Cold Molecules Research* (IOP - New Journal of Physics, **31**).

Carr, L. D., D. DeMille, R. V. Krems, and J. Ye (2009), New Journal of Physics **11** (5), 055049.

Cashen, M., and H. Metcalf (2001), Phys. Rev. A **63**, 025406.

Cashen, M., and H. Metcalf (2003), J. Opt. Soc. Am. B **20**, 915.

Chieda, M., and E. Eyler (2011), Phys. Rev. A **84**, 063401.

Chieda, M. A., and E. E. Eyler (2012), Phys. Rev. A **86**, 053415.

Chu, S., J. Bjorkholm, A. Ashkin, and A. Cable (1986), Phys. Rev. Lett. **57** (3), 314.

Chu, S., L. Hollberg, J. Bjorkholm, A. Cable, and A. Ashkin (1985), Phys. Rev. Lett. **55** (1), 48.

Cohen-Tannoudji, C., B. Diu, and F. Laloë (1977), *Quantum Mechanics* (Wiley, New York).

Corder, C., B. Arnold, X. Hua, and H. Metcalf (2015a), J. Opt. Soc. Am. B **32**, B75.

Corder, C., B. Arnold, and H. Metcalf (2015b), Phys. Rev. Lett. **114**, 043002.

Dai, D., Y. Xia, Y. Fang, L. Xu, Y. Yin, X. Li, X. Yang, and J. Yin (2015), Journal of Physics B: Atomic, Molecular and Optical Physics **48** (8), 085302.

Dalibard, J., and C. Cohen-Tannoudji (1989), J. Opt. Soc. Am. B **6** (11), 2023.

Doyle, J., B. Friedrich, R. V. Krems, and F. Masnou-Seeuws (2004), Eur. Phys. J. D **31** (2), 149.

Doyle, J. M., B. Friedrich, J. Kim, and D. Patterson (1995), Phys. Rev. A **52**, R2515.

Doyle, J. M., B. Friedrich, and E. Narevicius, Eds. (November 2016), *Cold Molecules, Special Issue of ChemPhysChem* **17** *3578 3825* (Wiley VCH).

Feynman, R., F. Vernon, and R. Hellwarth (1957), J. App. Phys. **28** (1), 49.

Fioretti, A., D. Comparat, A. Crubellier, O. Dulieu, F. Masnou-Seeuws, and P. Pillet (1998), Phys. Rev. Lett. **80**, 4402.

Freegarde, T., J. Walz, and T. Hänsch (1995), Optics Communications **117** (3), 262.

Frisch, R. (1933), Zeit. f. Phys. **86** (30), 42.

Galica, S. E., L. Aldridge, and E. E. Eyler (2013), Phys. Rev. A **88**, 043418.

Goepfert, A., I. Bloch, D. Haubrich, F. Lison, R. Schütze, R. Wynands, and D. Meschede (1997), Phys. Rev. A **56**, R3354.

Grimm, R., Y. Ovchinnikov, A. Sidorov, and V. Letokhov (1990), Phys. Rev. Lett. **65** (12), 1415.

Grimm, R., J. Söding, and Y. Ovchinnikov (1994), Opt. Lett. **19** (9), 658.

Grimm, R., G. Wasik, J. Söding, and Y. Ovchinnikov (1996), in *Proceedings of the Fermi School CXXXI*, edited by A. Aspect, W. Barletta, and R. Bonifacio (IOS Press, Amsterdam) p. 481.

Grove, T., B. Duncan, V. Sanchezvillicana, and P. Gould (1995), Phys. Rev. A **51** (6), R4325.

Gupta, R., C. Xie, S. Padua, H. Batelaan, and H. Metcalf (1993), Phys. Rev. Lett. **71** (19), 3087.

Hänsch, T., and A. Schawlow (1975), Opt. Commun. **13** (1), 68.

Hemmerling, B., E. Chae, A. Ravi, L. Anderegg, G. K. Drayna, N. R. Hutzler, A. L. Collopy, J. Ye, W. Ketterle, and J. M. Doyle (2016), Journal of Physics B: Atomic, Molecular and Optical Physics **49** (17), 174001.

Hua, X., C. Corder, and H. Metcalf (2016), Phys. Rev. A **93**, 063410.

Hulet, R. G., and D. Kleppner (1983), Phys. Rev. Lett. **51**, 1430.

Jayich, A. M., A. C. Vutha, M. T. Hummon, J. V. Porto, and W. C. Campbell (2014), Phys. Rev. A **89**, 023425.

Jessen, P., C. Gerz, P. Lett, W. Phillips, S. Rolston, R. Spreeuw, and C. Westbrook (1992), Phys. Rev. Lett. **69** (1), 49.

Kazantsev, A. P., and I. Krasnov (1989), J. Opt. Soc. Am. B **B6** (11), 2140.

Kazantzev, A. P. (1974), J. E. T. P. **39** (5), 784.

Lebedev, P. (1901), Ann. Phys. **6**, 433.

Lebedev, P. (1910), Astrophysical Journal **31**, 385.

Lett, P., K. Helmerson, W. Phillips, L. Ratliff, S. Rolston, and M. Wagshul (1993), Phys. Rev. Lett. **71** (14), 2200.

Lett, P., P. Julienne, and W. D. Phillips (1995), Annu. Rev. Phys. Chem. **46**, 423.

Lett, P., R. Watts, C. Westbrook, W. Philips, P. Gould, and H. Metcalf (1988), Phys. Rev. Lett. **61**, 169.

Liebisch, T. C., E. Blanshan, E. A. Donley, and J. Kitching (2012), Phys. Rev. A **85**, 013407.

Loy, M. M. T. (1974), Phys. Rev. Lett. **32** (15), 814.

Lu, T., X. Miao, and H. Metcalf (2005), Phys. Rev. A **71**, R 061405.

Lu, T., X. Miao, and H. Metcalf (2007), Phys. Rev. A **75**, 063422.

Marx, S., D. Adu Smith, G. Insero, S. A. Meek, B. G. Sartakov, G. Meijer, and G. Santambrogio (2015), Phys. Rev. A **92**, 063408.

Metcalf, H. (2008), Phys. Rev. A **77**, R 061401.

Metcalf, H., and P. van der Straten (1999), *Laser Cooling and Trapping* (Springer, New York).

Miao, X., E. Wertz, M. G. Cohen, and H. Metcalf (2007), Phys. Rev. A **75**, 011402.

Miller, J., R. Cline, and D. Heinzen (1993), Phys. Rev. Lett. **71** (14), 2204.

Mulser, P. (1985), J. Opt. Soc. Am. B **2** (11), 1814.

Neuhauser, W., M. Hohenstatt, P. Toschek, and H. Dehmelt (1978), Phys. Rev. Lett. **41**, 233.

Nichols, E. F., and G. F. Hull (1903), Phys. Rev. **17**, 26.

Nölle, B., H. Nölle, J. Schmand, and H. J. Andrä (1996), Europhysics Letters **33**, 261.

Partlow, M., X. Miao, J. Bochmann, M. Cashen, and H. Metcalf (2004), Phys. Rev. Lett. **93**, 213004.

Petra, S., L. Feenstra, W. Hogervorst, and W. Vassen (2004a), App. Phys. B **78**, 133.

Petra, S., K. A. H. van Leeuwen, L. Feenstra, W. Hogervorst, and W. Vassen (2004b), App. Phys. B **79**, 279.

Phillips, W., and H. Metcalf (1982), Phys. Rev. Lett. **48** (9), 596.

Phillips, W. D. (1998), Rev. Mod. Phys. **70**, 721.

Picqué, J.-L., and J.-L. Vialle (1972), Opt. Commun. **5**, 402.

Prodan, J., W. Phillips, and H. Metcalf (1982), Phys. Rev. Lett. **49**, 1149.

Rabi, I. (1937), Phys. Rep. **51**, 652.

Reeves, J. (2010), *Neutral Atom lithography Using the 389 nm Transition in Metastable Helium*, Ph.D. thesis (Stony Brook University).

Romanenko, V., A. Romanenko, and L. Yatsenko (2016), Ukr. J. Phys. **61**, 309.

Romanenko, V. I., and L. P. Yatsenko (2011), J. Phys. B **44**, 115305.

Rubbmark, J. R., M. M. Kash, M. G. Littman, and D. Kleppner (1981), Phys. Rev. A **23**, 3107.

Salomon, C., J. Dalibard, A. Aspect, H. Metcalf, and C. Cohen-Tannoudji (1987), Phys. Rev. Lett. **59**, 1659.

Sawicki, D., and J. H. Eberly (1999), Optics Express **4**, 217.

Schieder, R., H. Walther, and L. Wöste (1972), Opt. Commun. **5**, 337.

Sheehy, B., S. Shang, P. van der Straten, S. Hatamian, and H. Metcalf (1990), Phys. Rev. Lett. **64** (8), 858.

Shuman, E. S., J. F. Barry, D. R. Glenn, and D. DeMille (2009), Phys. Rev. Lett. **103**, 223001.

Söding, J., R. Grimm, Y. Ovchinnikov, P. Bouyer, and C. Salomon (1997), Phys. Rev. Lett. **78** (8), 1420.

Stack, D., J. Elgin, P. M. Anisimov, and H. Metcalf (2011), Phys. Rev. A **84**, 013420.

van der Straten, P., and H. Metcalf (2016), *Atoms and Molecules Interacting with Light* (Cambridge University Press, Cambridge CB2 8BS, UK).

Ungar, P., D. Weiss, S. Chu, and E. Riis (1989), J. Opt. Soc. Am. B **6** (11), 2058.

Voitsekhovich, V., M. Danileiko, A. Negriiko, V. Romanenko, and L. Yatsenko (1988), Zh. Tekh. Fiz. **58** (6), 1174, [Sov. Phys. Tech. Phys. **33**, 690-691, (1988)].

Voitsekhovich, V., M. Danileiko, A. Negriiko, V. Romanenko, and L. Yatsenko (1989), Pisma Zhur. Teor. Eksp. Fiz. **49** (3), 138, [JETP Lett. **49**, 161-164, (1989)].

Weinstein, J., R. deCarvalho, T. Guillet, B. Friedrich, and J. Doyle (1998), Nature **395**, 148.

Williams, C., and P. Julienne (1994), J. Chem. Phys. **101** (3), 2634.

Williams, M., F. Chi, M. Cashen, and H. Metcalf (1999), Phys. Rev. A **60**, R1763.

Williams, M., F. Chi, M. Cashen, and H. Metcalf (2000), Phys. Rev. A **61**, 023408.

Wineland, D., and H. Dehmelt (1975), Bull. Am. Phys. Soc. **20**, 637.

Wineland, D., R. Drullinger, and F. Walls (1978), Phys. Rev. Lett. **40**, 1639.

Yang, X., C. Li, Y. Yin, S. Xu, X. Li, Y. Xia, and J. Yin (2017), Journal of Physics B: Atomic, Molecular and Optical Physics **50** (1), 015001.

Yatsenko, L., and H. Metcalf (2004), Phys. Rev. A **70**, 063402.

Zhelyazkova, V., A. Cournol, T. E. Wall, A. Matsushima, J. J. Hudson, E. A. Hinds, M. R. Tarbutt, and B. E. Sauer (2014), Phys. Rev. A **89**, 053416.

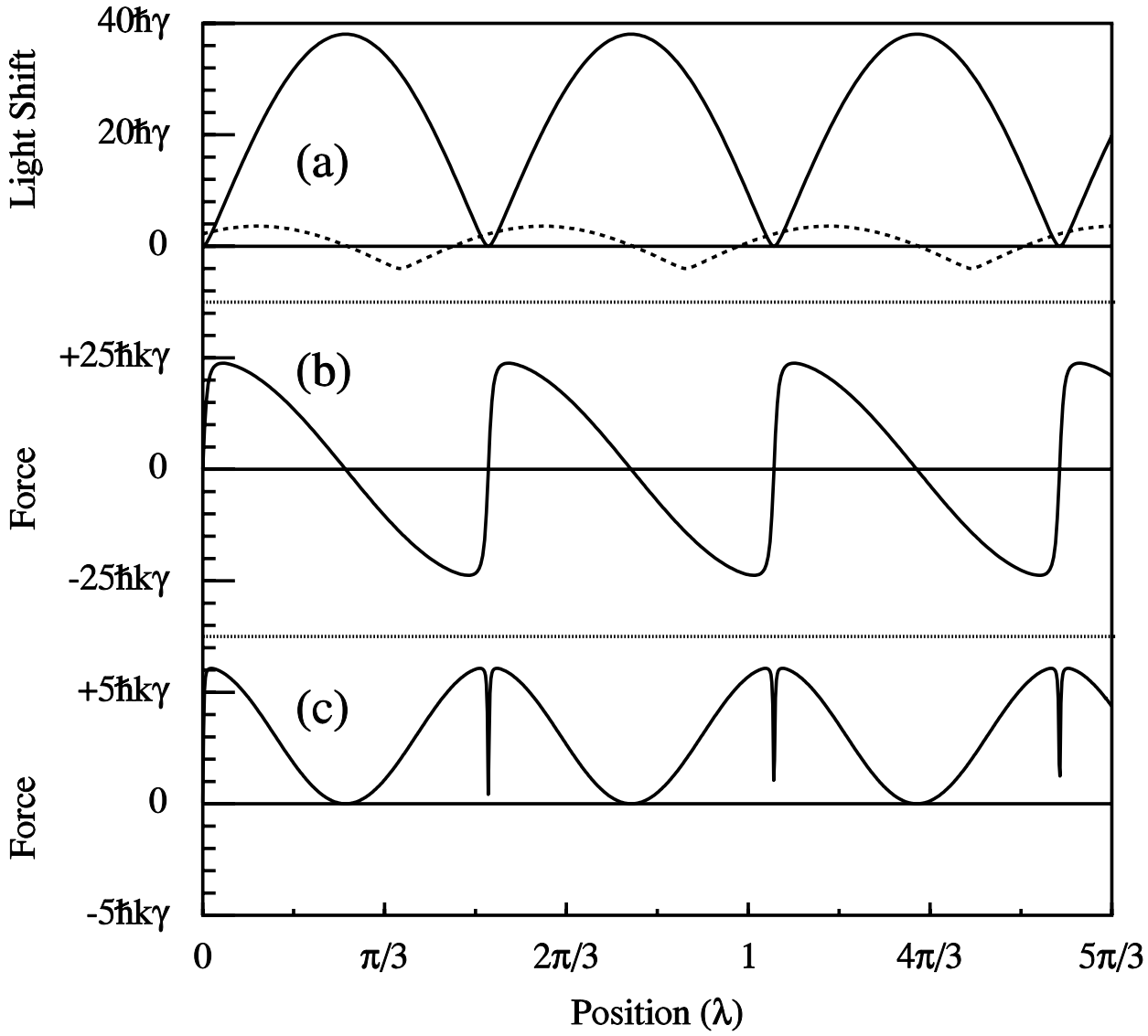

FIG. 2 Scheme for the rectification of the dipole force. The solid curve in (a) shows the light shift of the ground state of a two level atom in the standing wave of field 1, $\Omega_1 = 40\gamma$ and $\delta = 3\gamma$. Note that it is not sinusoidal because $\Omega \gg \delta$ (Metcalf and van der Straten, 1999). The dotted curve shows the spatial variation of the detuning caused by the smaller light shift of field 2 that has $\delta_2 = 50\gamma$ and $\Omega_2 = 200\gamma$. Part (b) shows the gradient of the curve in (a), corresponding to the force on a ground state atom from field 1. Part (c) shows the total rectified force on the atoms because the sign of the detuning reverses appropriately. Simply taking minus the gradient of the curve in (a) is not appropriate because the atom spends considerable time in the excited state whose light shift is opposite, so it is necessary to calculate $< F >= -\mathrm{tr}(\rho \nabla \mathcal{H})$. Thus choosing the relative spatial phase of these standing waves carefully results in a rectification of the force. (Figure from (Metcalf and van der Straten, 1999).)

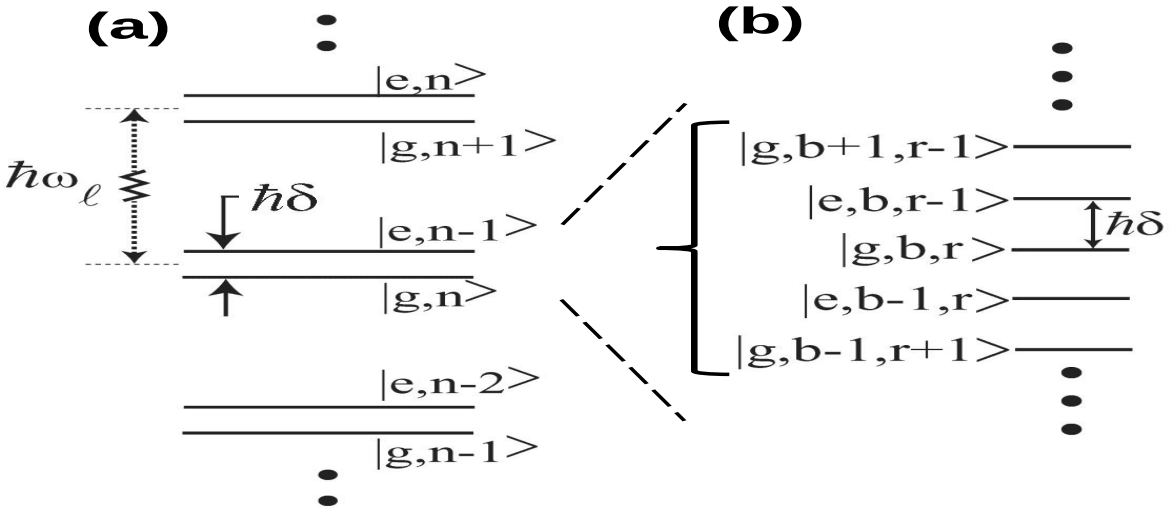

FIG. 4 Part (a) shows the familiar dressed state pairs of an atom in a single frequency light field at ω_ℓ, detuned below atomic resonance, ω_a ($\delta < 0$). Interaction with the light field of quantum number n mixes these bare states $|e, n-1\rangle$ and $|g, n\rangle$ to form new states split by $\hbar\omega_{ds}$ (not shown) found from Eq. 2. Part (b) shows that with two frequencies, and hence two field quantum numbers r and b, there arises a ladder of energy states both up and down from each original dressed state pair (Fig. adapted from (Yatsenko and Metcalf, 2004)).

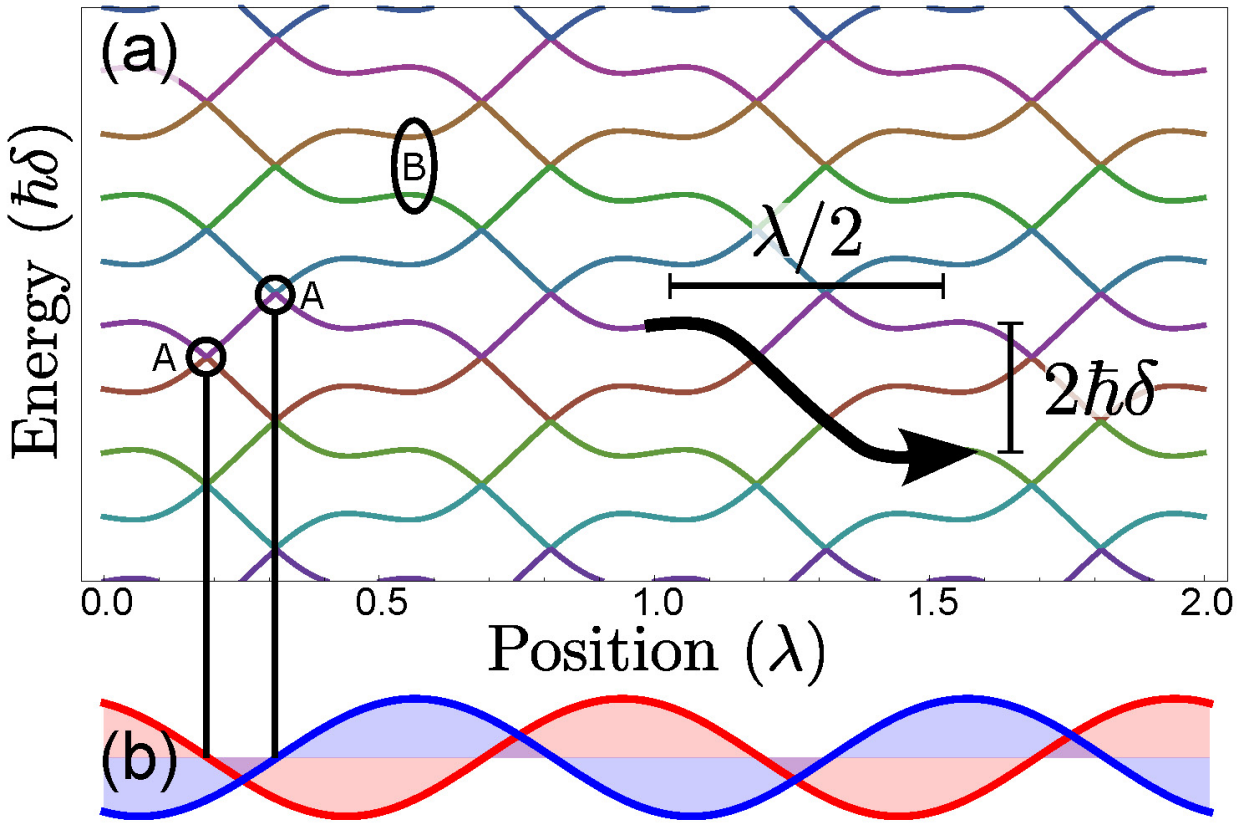

FIG. 5 The eigenvalues of the two-frequency dressed state system separated by $\hbar\delta$ where the two fields have equal strength but spatial phase offset of $\lambda/8$, along with a typical path followed by an atom moving to the right. The light field comprises bichromatic standing waves so that the intensities vary with position. The right choice of parameters produces exact crossings at points (A) because one of the standing wave fields has a node. Moving atoms can make Landau-Zener transitions and cross from one energy manifold to another, as shown by the heavy arrow, thereby exchanging optical potential energy for kinetic energy (Figure from (Corder *et al.*, 2015b)).

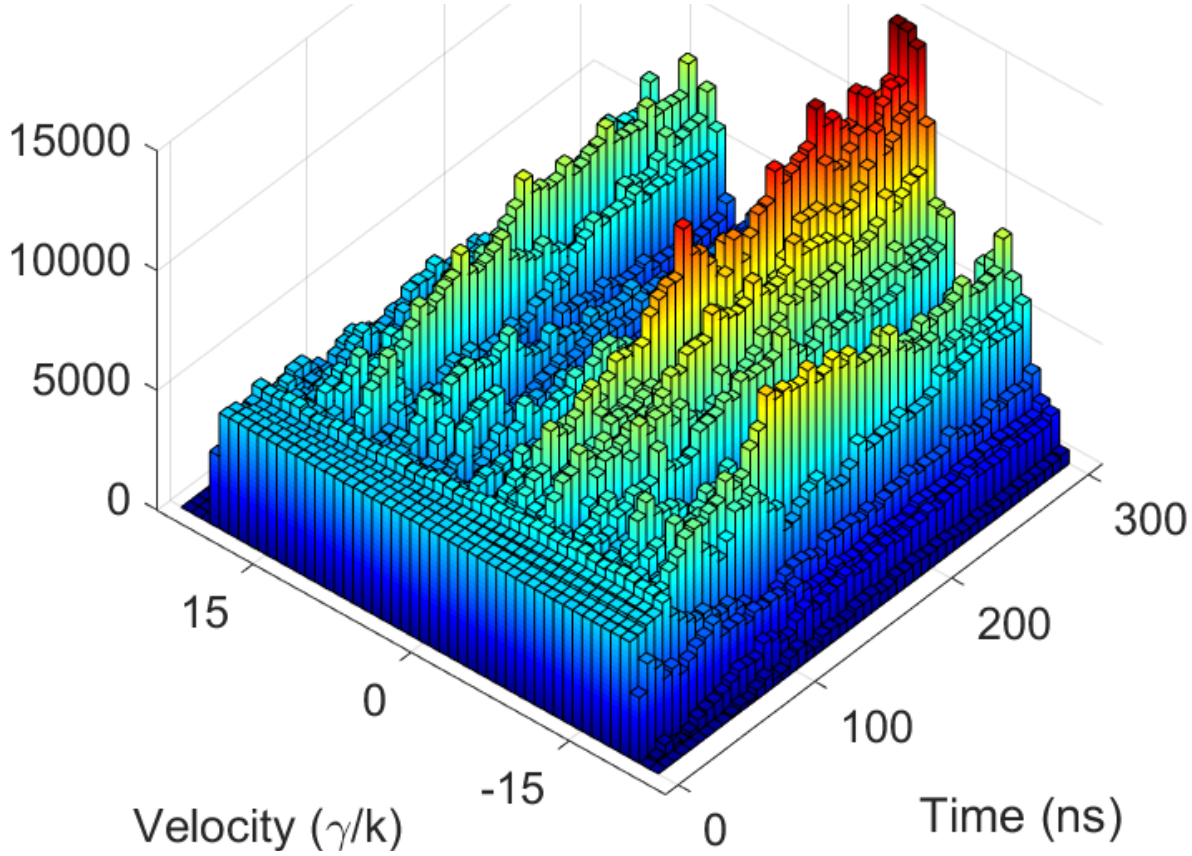

FIG. 6 This shows a simulation of the time evolution of the velocity space density of an ensemble of atoms that started with a uniform array of initial velocities (Hua *et al.*, 2016). Here $\delta = 15\gamma$ and there is a strong accumulation of atoms at speed $-v_c = -7.5\,\gamma/k$. Behind this high ridge is a deep valley of width $\sim 15\gamma/k \approx 35 v_r$ where the atoms began. This simulation was done for the $2^3\mathrm{S} \rightarrow 3^3\mathrm{P}$ transition in He at $\lambda = 389$ nm where $\omega_r \approx 330$ kHz so that $t_c \approx 380$ ns. Even at $t = t_c/2 \approx 190$ ns there is evidence of substantial cooling. (Figure from (Hua *et al.*, 2016).)

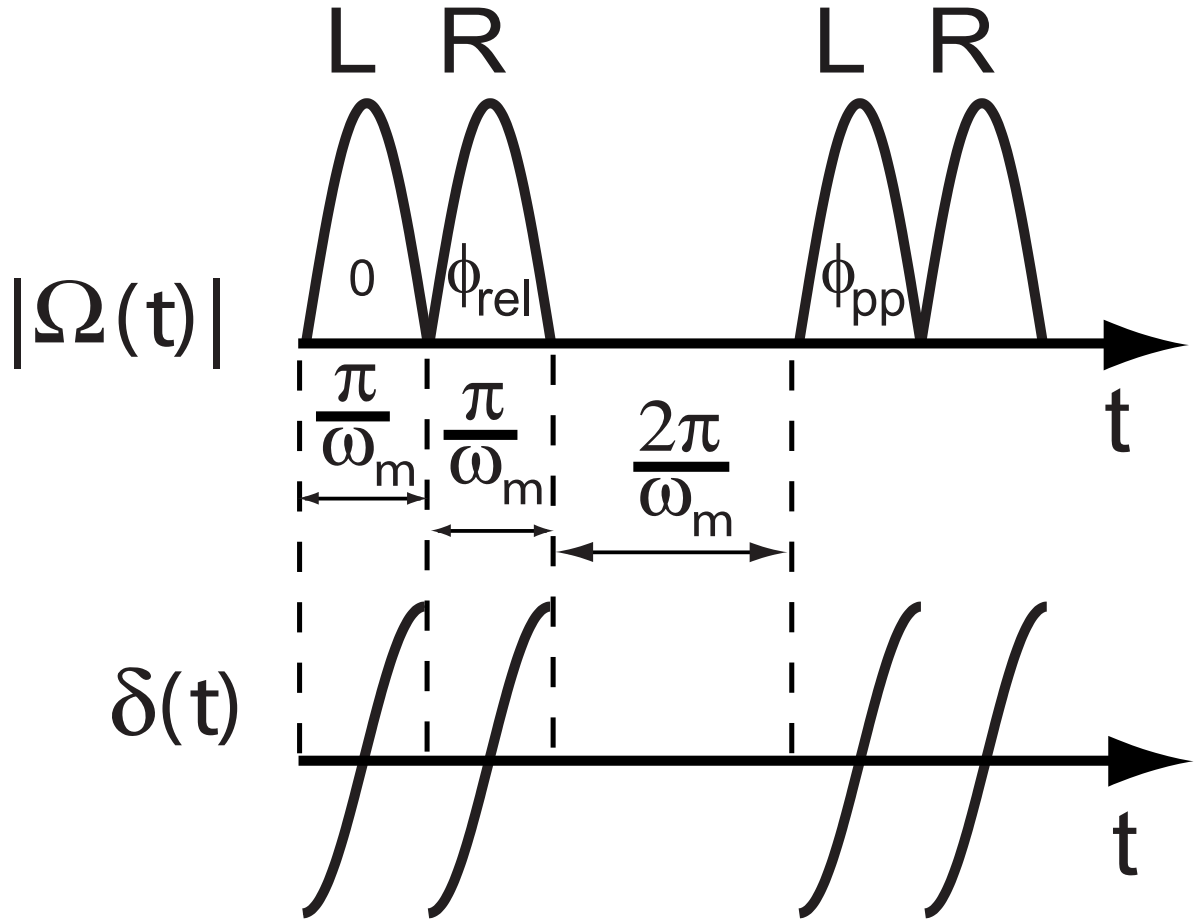

FIG. 7 The upper portion shows two pulse pairs with a gap between them. The gap is for experimental reasons and the phase notations will be discussed later. The lower part shows the frequency sweeps, and in this case they are both upward. However, they can be reversed or even in opposite directions. (Figure from (Stack *et al.*, 2011))

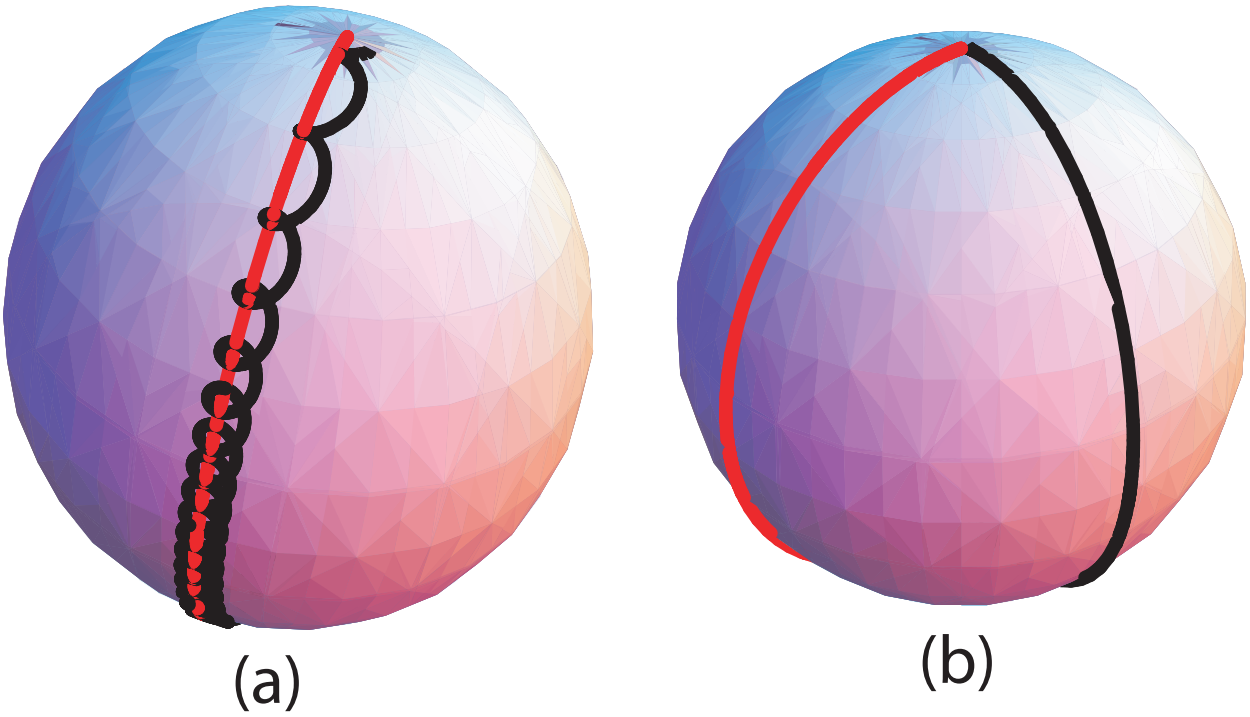

FIG. 8 Part (a) shows the arc of a smoothly swept $\vec{\Omega}(t)$ as the detuning varies from one side of resonance to the other (red curve - smooth) using $\delta_0 = 30\,\omega_m$ and $\Omega_0 = 50\,\omega_m$. It begins at one pole where $\Omega(0) \ll \delta(0) = \delta_0$ so that $\vec{\Omega}(0)$ is nearly polar, arcs toward the equator where $\delta(t) = 0$ and $\Omega(t) = \Omega_0$, and finishes at the other pole at the end of the pulse where $\Omega(t)$ is again very small. Here $\vec{R}$ (black curve) makes many precession cycles and stays close to $\vec{\Omega}(t)$ during the sweep. Part (b) has $\delta_0 = 1.10\,\omega_m$ and $\Omega_0 = 1.61\,\omega_m$ to show an unusual case where the trajectory of $\vec{R}$ is a simple arc along a meridian that is $\sim 90°$ away from the path of $\vec{\Omega}(t)$ so that $\vec{R}$ also goes from pole to pole (Figure adapted from Ref's. (Miao *et al.*, 2007; Stack *et al.*, 2011)).

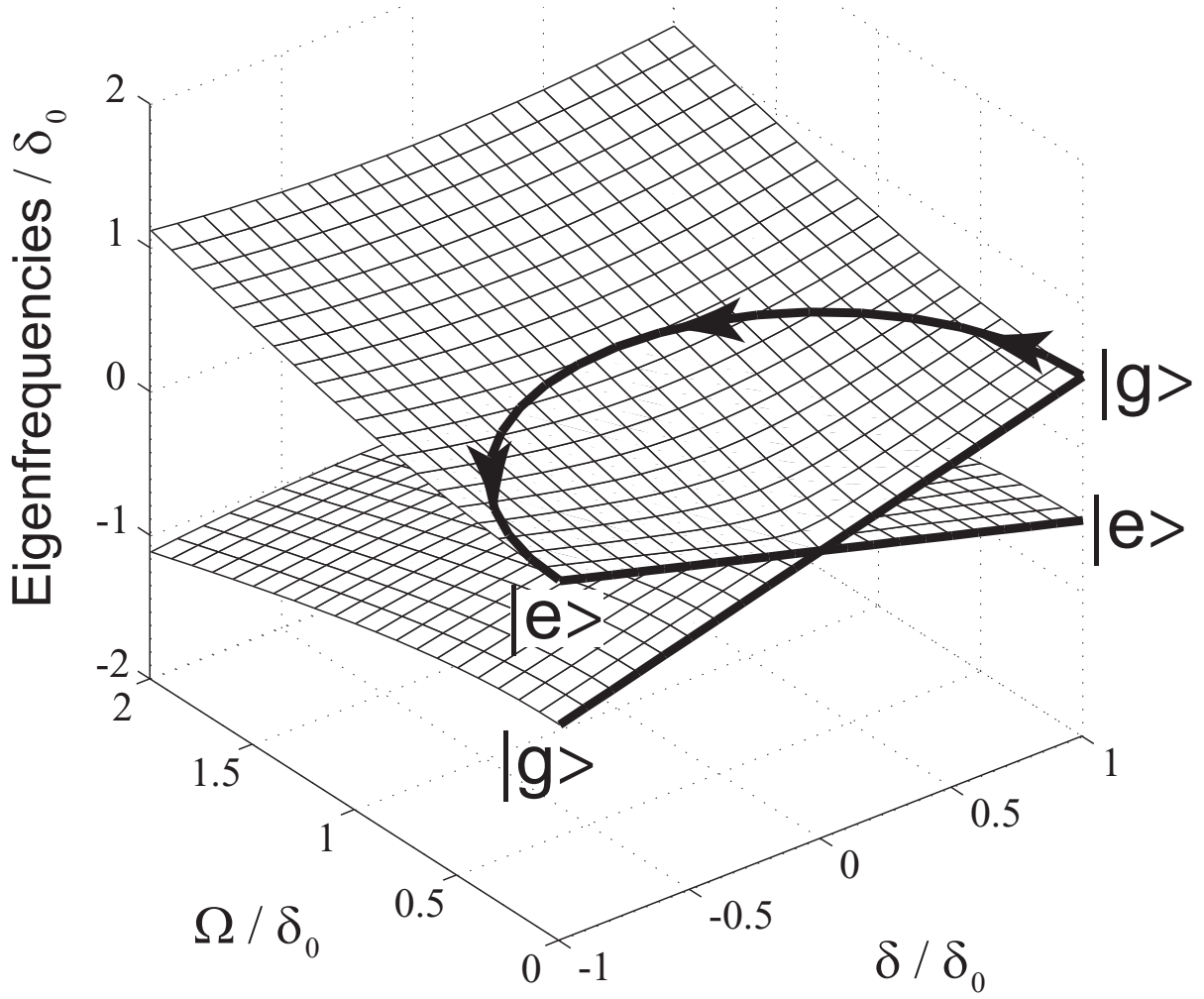

FIG. 9 A plot of Eq. 2. The $|g, n\rangle$ and the $|e, n-1\rangle$ dressed states comprise two separated energy sheets except at their conical intersection at the origin. Their upper (lower) state is ground at $\Omega = 0$ for $\delta > 0$ ($\delta < 0$). The indicated path is a possible trajectory for ARP. (Fig. from (Lu *et al.*, 2005))

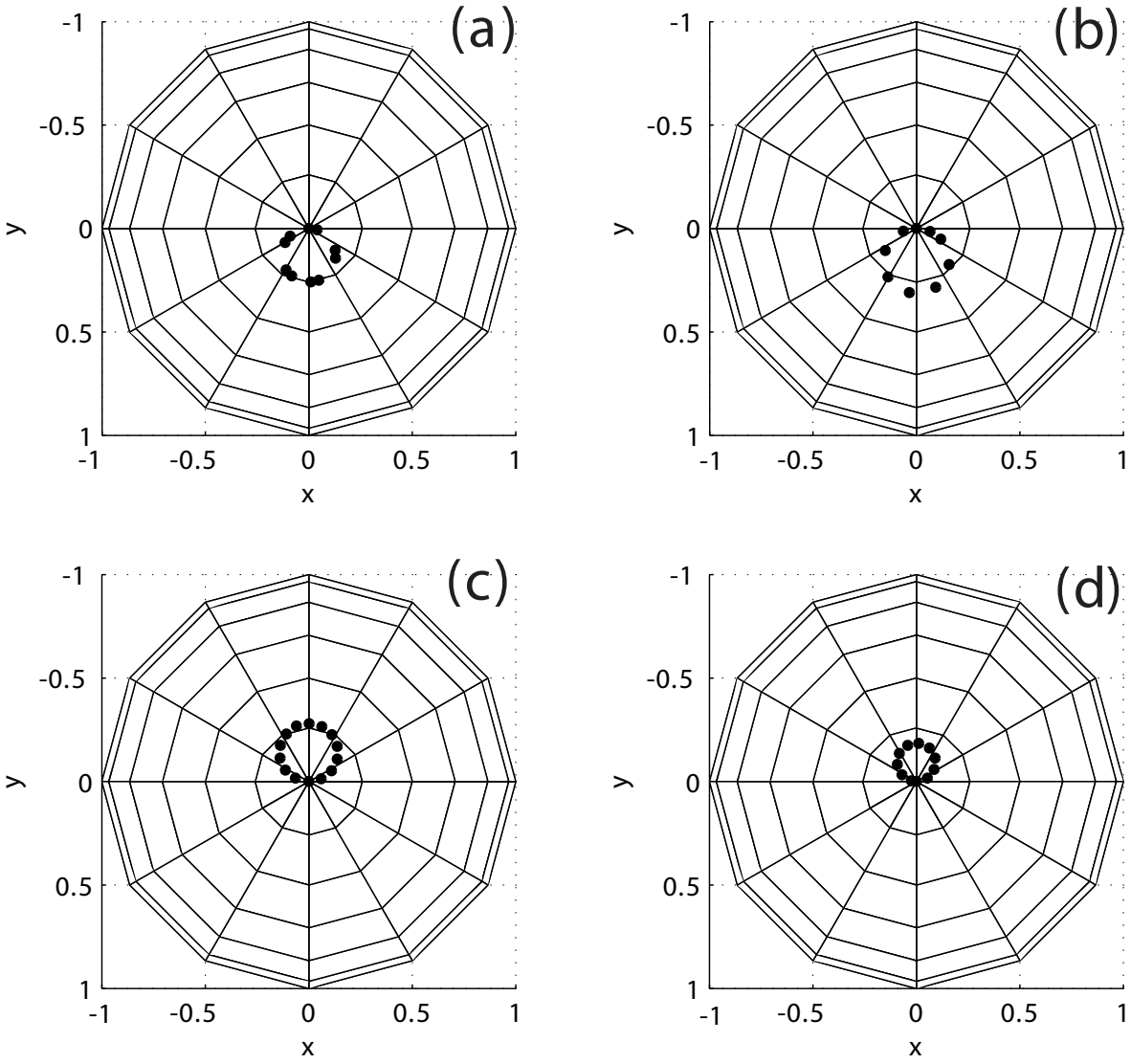

FIG. 10 Plots showing calculated values of $\vec{R}$ on the Bloch sphere as viewed from the South pole. Each set of points lies on a circle whose radius and center depend on the sweep parameters. These parameters are $(\delta_0/\omega_m, \Omega_0/\omega_m)$ = (a) - (2.4, 1.8), (b) - (3, 4.4), (c) - (7, 7), and (d) - (14, 18). The points appear to be not evenly spaced (*e.g.,* part (a)) because the rotation angle is large and more than one full rotation is shown. (Fig. from (Lu *et al.*, 2005))

.

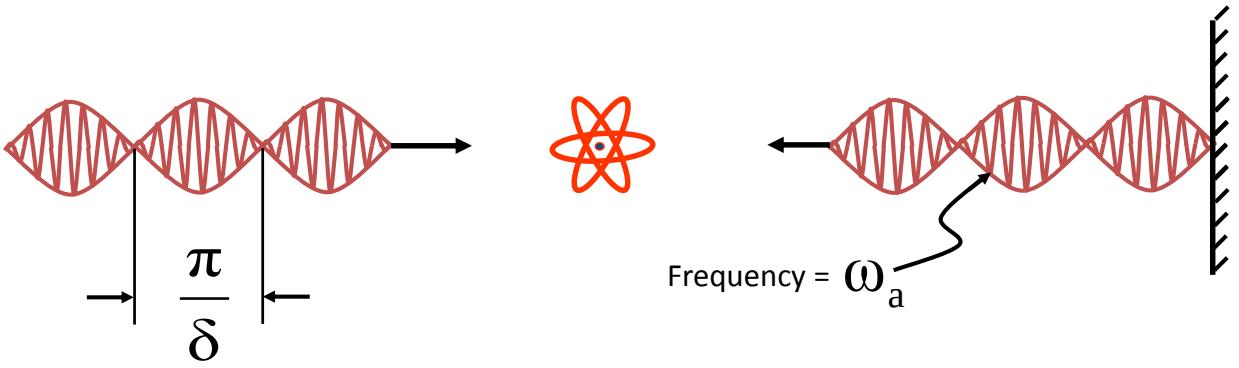

FIG. 11 Counter-propagating beams, each carrying two frequencies. The frequencies are equally displaced from ω_a, the atomic frequency, so that the carrier is on resonance. The beat between these frequencies produces the "pulses" that are used in the π-pulse model of the BF.

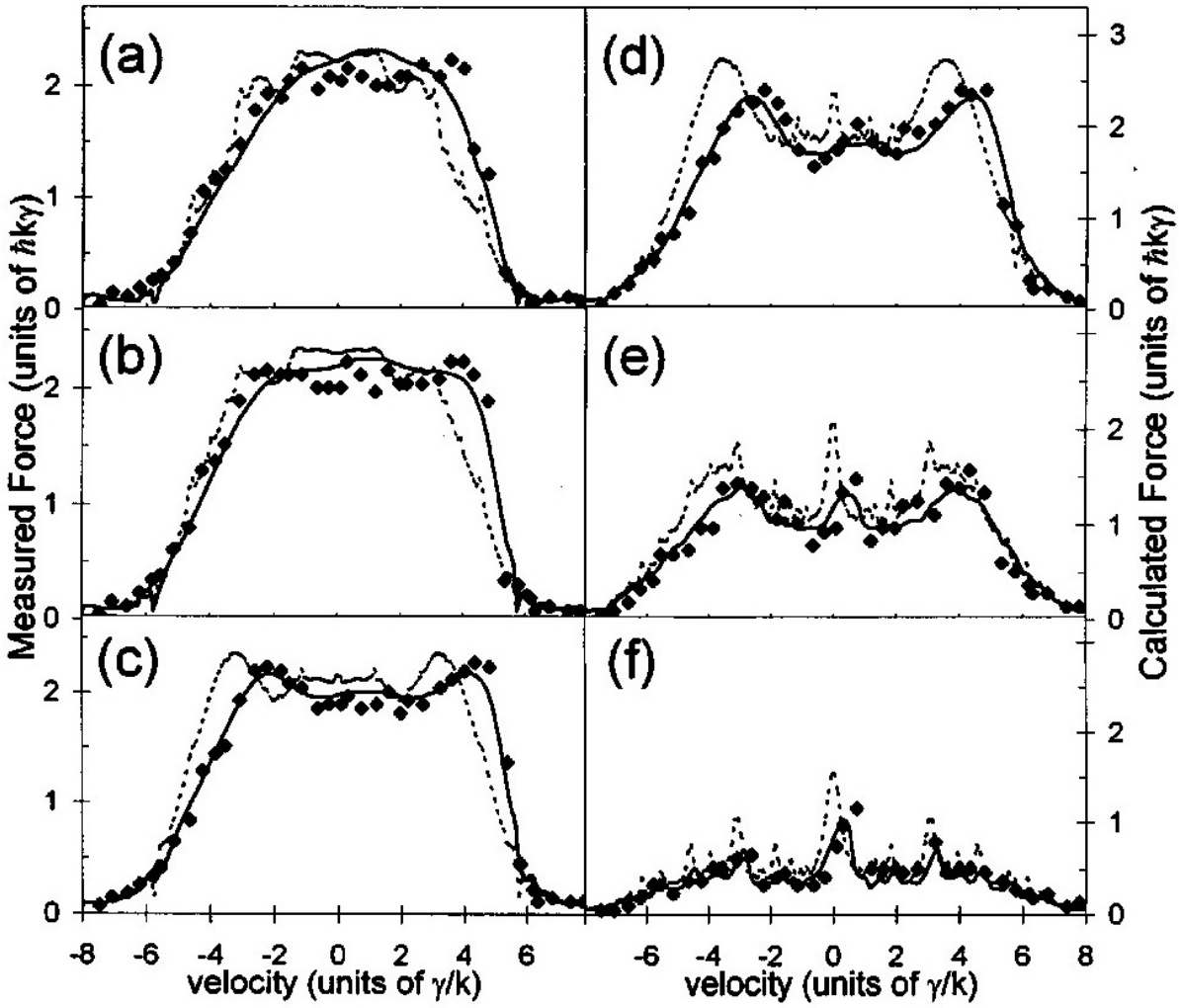

FIG. 12 Each panel shows the velocity dependence of the bichromatic force calculated for a relative spatial phase offset of 5% larger than $\lambda/8$ (95^o) by direct numerical integration of the OBEs (dotted line), the calculated values convolved with the experimental resolution (solid line), and the measured values (data points). These measurements and calculations were done with $\delta = 2\pi \times 55$ MHz $= 9.1\gamma$. The different values of Ω/δ were set using a half-wave plate and polarizer combination, starting with 1.19 in (a), 1.13 in (b), 1.07 in (c), 0.98 in (d), 0.88 in (e), and 0.76 in (f). The calculated and experimental plots have vertical scales different by the factor 0.83 in all panels. (Fig. from (Williams *et al.*, 1999).)

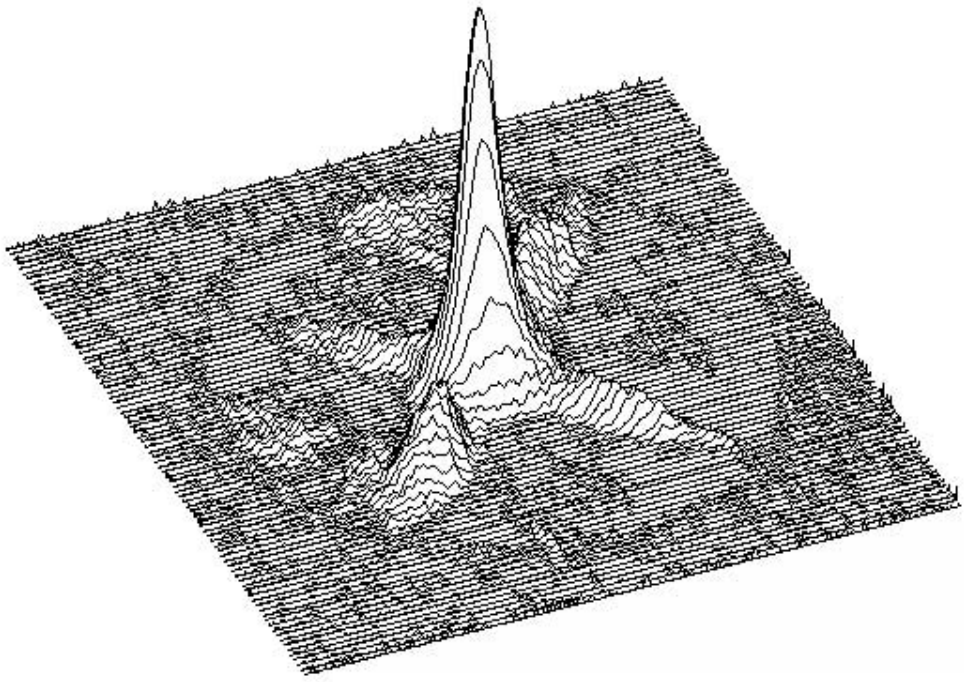

FIG. 13 Profile of the collimated He* beam. Atoms could be captured from 180 mrad (2 × FWHM) into this 7.5 mrad FWHM peak. The intensity was nearly 10^{10} atoms/s-mm^2 and the brightness was 10^{16} atoms/s-sr-mm^2. The BF detuning was $2\pi\times$ 60 MHz. (Figure from (Partlow *et al.*, 2004).)

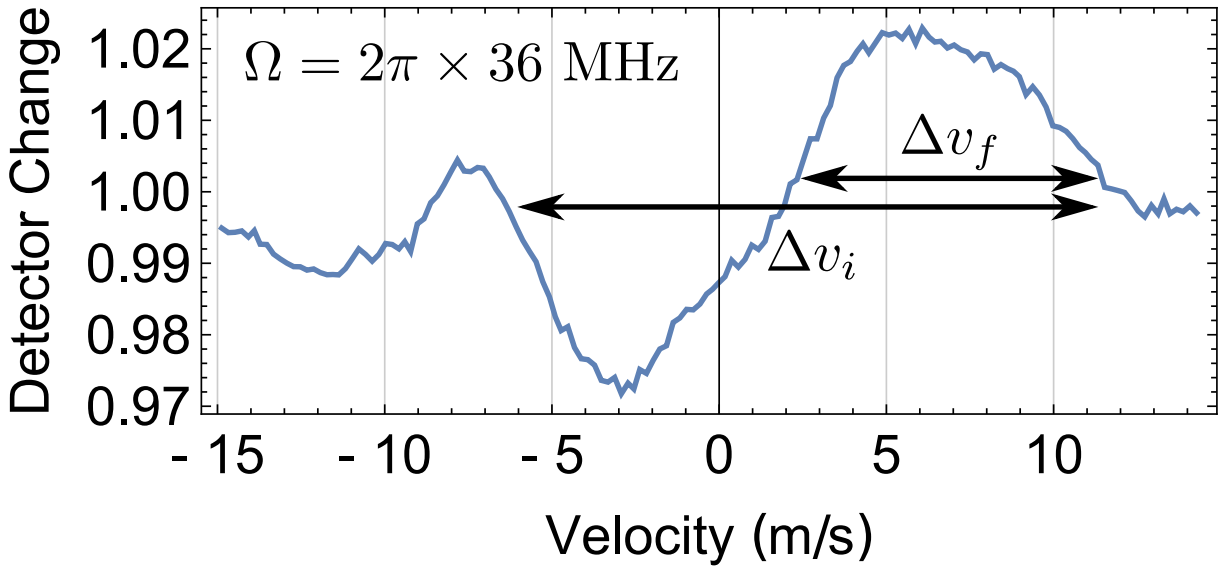

FIG. 14 Plot of the atomic distribution measured 63 cm downstream from the interaction region after an average cooling time of 220 ns. The Rabi frequency was $\Omega = 2\pi \times 36$ MHz, a compromise between two optimum values (see Ref. (Corder *et al.*, 2015a)). There is a large background from the He* source so the raw data here shows a change of only a few percent. The velocity smearing caused by the width of the longitudinal velocity distribution is a few m/s, but it affects only the deflected atoms. It does not affect the width of the "hole" because there are no atoms there. (Figure adapted from Ref. (Corder *et al.*, 2015b).)

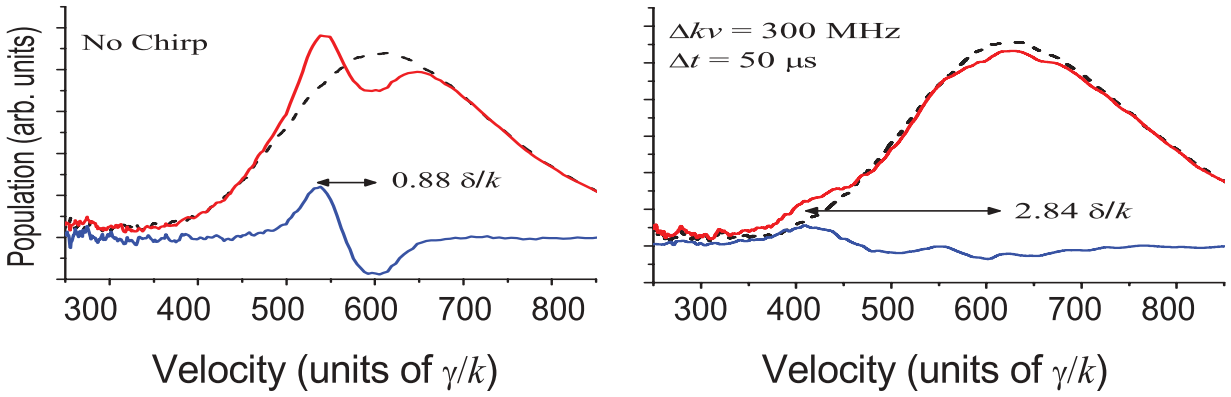

FIG. 15 Observed slowing of a He* beam with chirped light using the BF with $\delta = 74\gamma$ and $\Omega = \sqrt{3/2}\,\delta$. The left panel shows the result with no chirp (fixed δ), and the right panel shows the result of chirping the center frequency by 300 MHz. The velocity range is very much larger in the latter case. The dotted curve shows the original velocity distribution, the red curve near it shows the change one, and the blue curve (lowest one) is their difference. (Figure adapted from (Chieda and Eyler, 2012).)

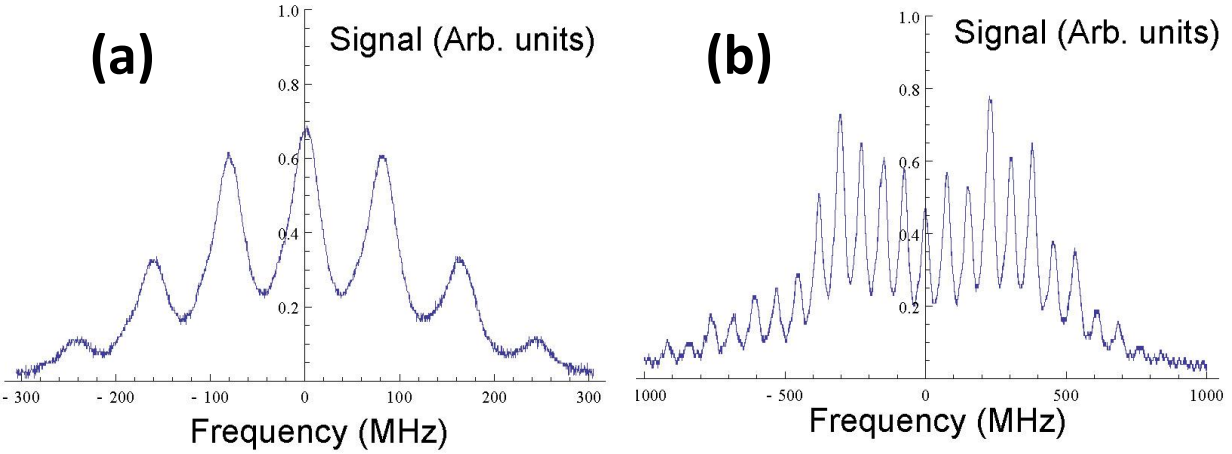

FIG. 16 Part (a) shows the frequency spectrum of the amplitude-modulated light with no phase modulation and part (b) shows the frequency spectrum of the light with both phase and amplitude modulation (note the difference in scales). (Figure adapted from (Miao *et al.*, 2007)).

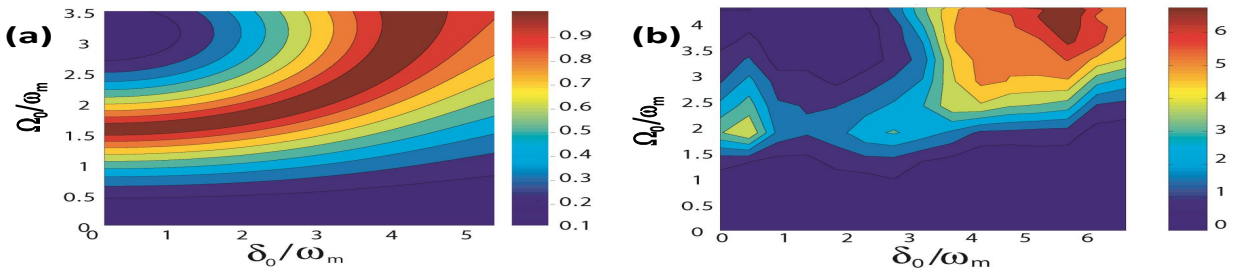

FIG. 17 Part (a) shows the dependence of the ARP force on the peak Rabi frequency Ω_0 and the range of the frequency sweep $\pm\delta_0$, calculated from the solutions of Eq. 6, and using the Ehrenfest theorem (see (Lu *et al.*, 2005)). Part (b) shows the results of measuring the ARP force over a similar region of parameter space as part (a). The agreement in the strength of the force is qualitatively good, and quantitatively acceptable except for a numerical factor slightly larger than 2. (Figure from (Miao *et al.*, 2007).)